Radiation Belt Dynamics and Remote Sensing of the Earth's Plasmasphere

International School of Space Science

26-30 September 2022

Interaction of radiation belt energetic particles with VLF hiss

J.-F. Ripoll [1,2]

(jean-francois.ripoll@cea.fr)

1 CEA, DAM, DIF, Arpajon, France

2 UPS, CEA, LMCE, France

DE LA RECHERCHE À L'INDUSTRIE

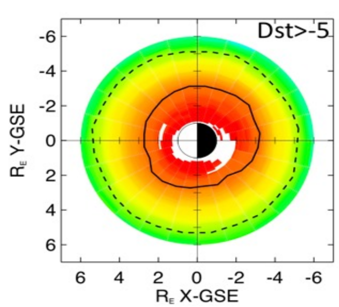

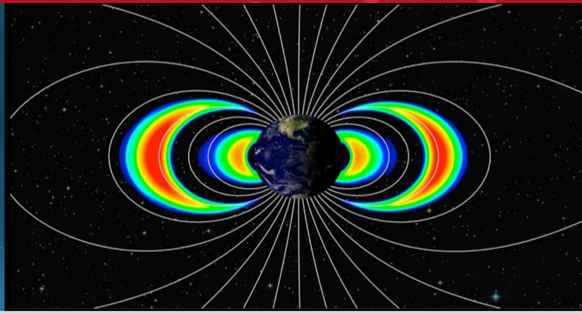

Science content of the course

1- Information from textbooks and seminal articles (cited throughout the course)

2- New results from recent articles conducted by the author and his collaborators

3- Use of observations from NASA Van Allen Probes to illustrate the claims (some unpublished yet)

Collaborators of the studies:

V. Loridan[1], G. Cunningham[2], M. Denton[3,4], O. Santolík[5,6], D. Malaspina[7], S. Thaller[10], G. Reeves[2,3], D. Hartley[8], W. S. Kurth[8], C. A. Kletzing[8], D. L. Turner[10], J. F. Fennell[9], M. G. Henderson[2], A. Y. Ukhorskiy[10,] A. Y. Drozdov[11], Y. Y. Shprits[12,13], J.S Cervantes Villa[13], E. Botek[14], V. Pierrard[14,15], M. Cosmides[1]

1 CEA, DAM, DIF, Arpajon, France
2 Los Alamos National Laboratory
3 New Mexico Consortium
4 Space Science Institute, Boulder
5 Academic Science Czech Republic
6 Charles University, Prague
7 LASP
8 University of Iowa
9 Aerospace Corporation
10 Applied Physics Laboratory
11 University of Minnesota
12 UCLA
13 Helmholtz Centre Potsdam, GFZ
14 BIRA, Belgium,
15UC Louvain, Belgium

Outlines

Introduction

Observations of the ambient environment:

1- Cold plasma density (briefly)

2- Whistler-mode waves (hiss focus)

Observations of the radiation belts

Event-driven wave-particle interactions and QL Fokker-Planck simulations of the radiation belts

Conclusions and Perspectives

Introduction

Earth’s Radiation Belts: sketch and fundamental role of hiss

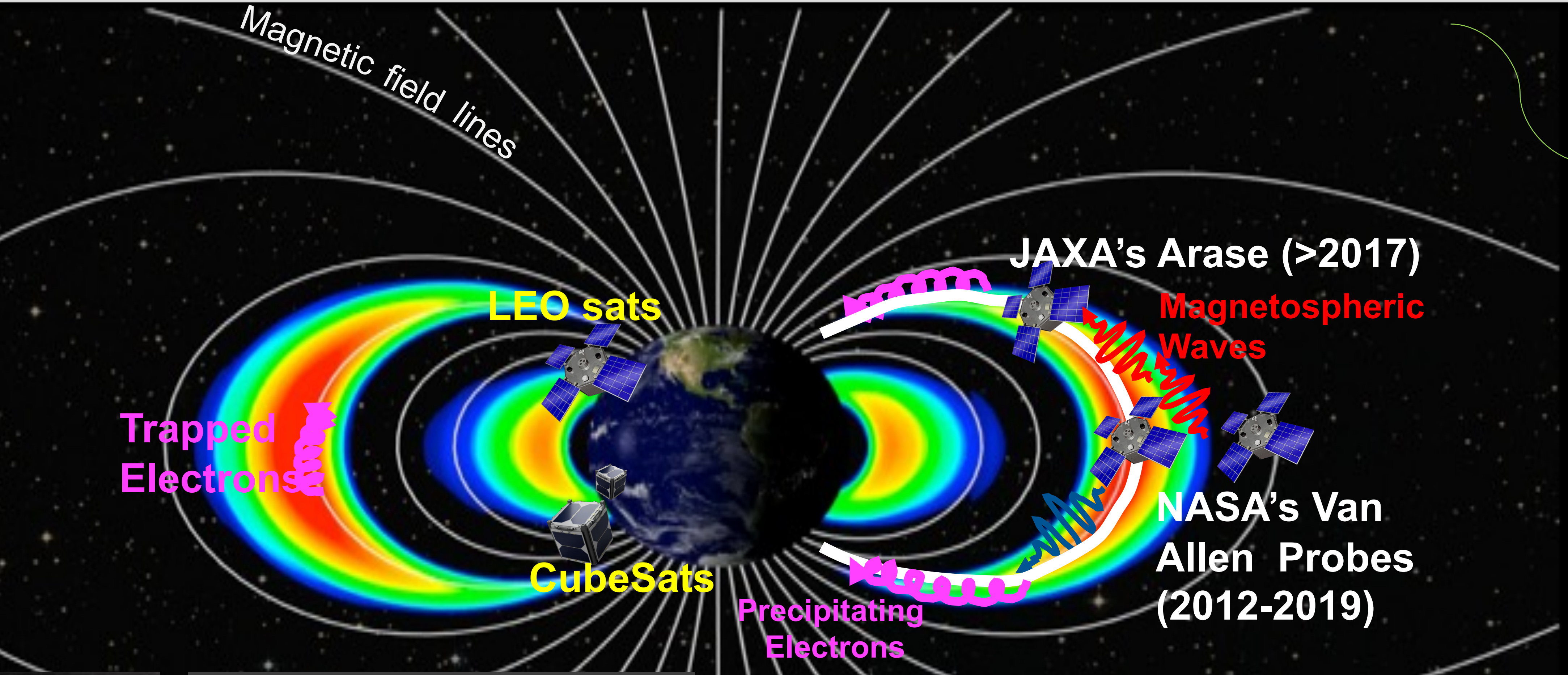

J. Pickering, J. van Allen, W. von Braun

- Discovered in 1958, by James Van Allen
- First US satellite, Explorer I
- Discovered by accident
- Intended to measure cosmic rays
- But count rates were too high

issibern.ch/teams/radbeltphysics/

Radiation Belt Physics From Top To Bottom: Combining Multipoint Satellite Observations And Data Assimilative Models To Determine The Interplay Between Sources And Losses

ISSI Team led by J.-F. Ripoll (FR), G. D. Reeves (US) & D. L. Turner (US)

Earth's Radiation Belts: sketch and fundamental role of hiss

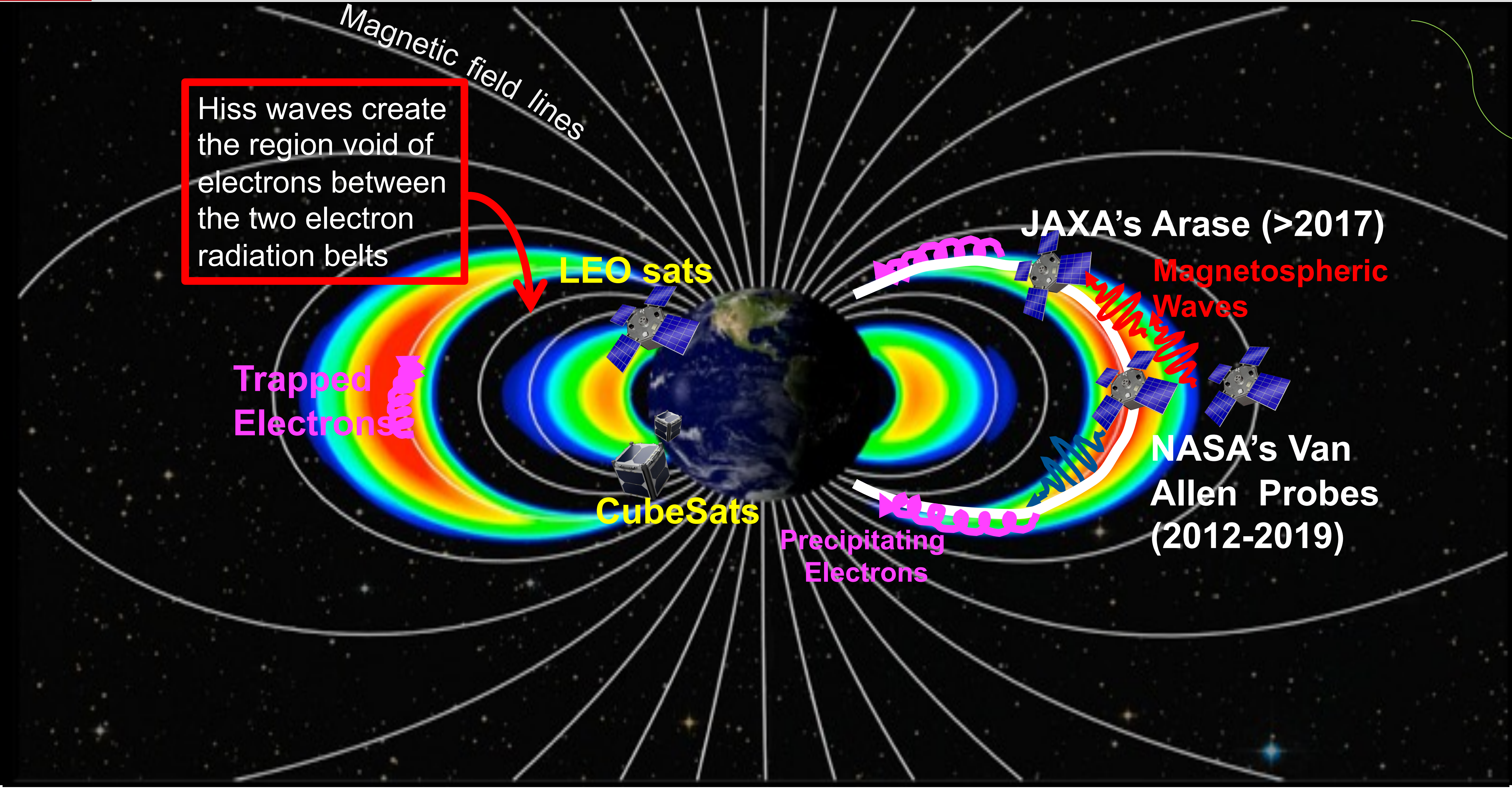

The NASA Van ALLEN Probes mission: a mission build to study the radiation belts

Two satellites launched (A+B) on 08/30/2012 and ended in 07/2019 (RBSP-B) and 10/2019 (RBSP-A)
~600 M$ mission

Courtesy, S. Ukhorskiy, JHU-APL

Among the main NASA mission objectives:

- Better understand radiation belt physics
- Validate a wide range of models
- Explain x10 difference between simulations & observations

How to

- Using 2 s/c measuring the ambient environment and the radiation belts fluxes
- Measure ambient EM waves to solve for wave-particle interactions

The NASA Van ALLEN Probes mission: measurements of ambient particles and electromagnetic waves + energetic radiation belts particles

Instrument suits for plasma (P), waves (W), and fields (F)

RBSPICE

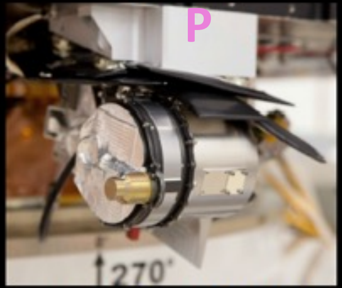

e, H, He, O: 1 keV-2 MeV

REPT

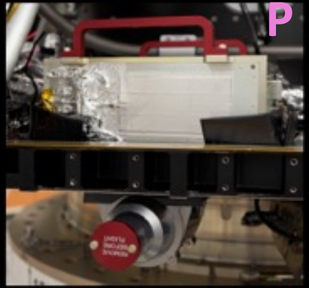

e: 2-10 MeV, H: 10-100 MeV

HOPE

e, H, He, O: 1 eV-50 keV

EMFISIS

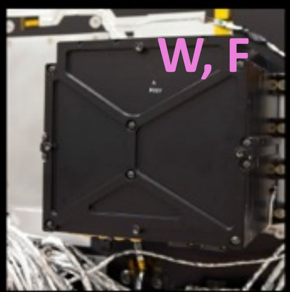

B, E (>10 Hz)

EFW

E (<100 Hz)

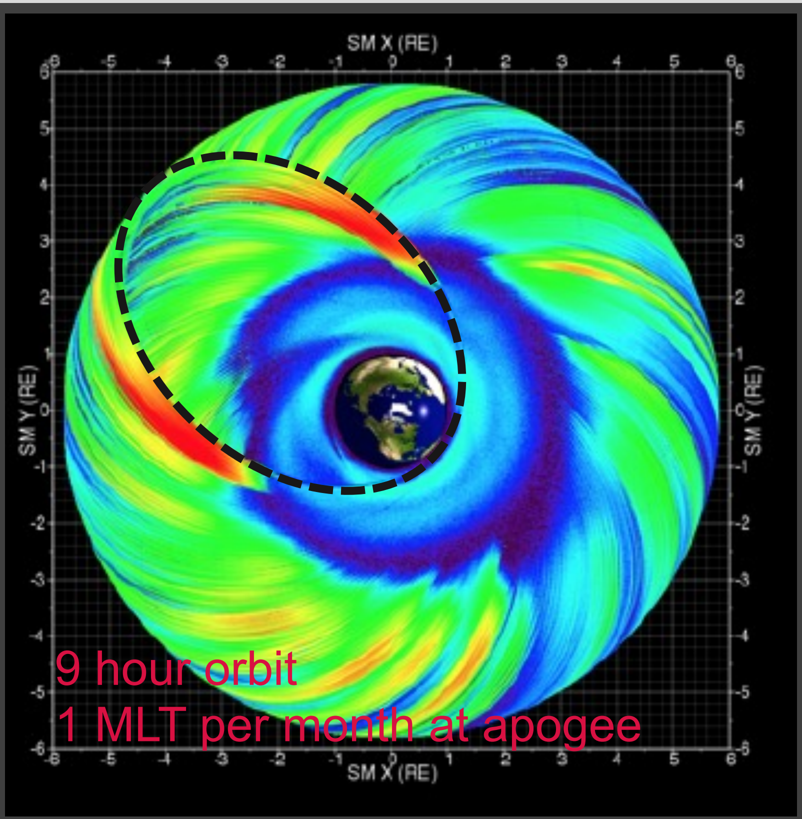

Courtesy, S. Ukhorskiy, JHU-APL

Tdrift(1 MeV, 90°,L=6)~10 mins

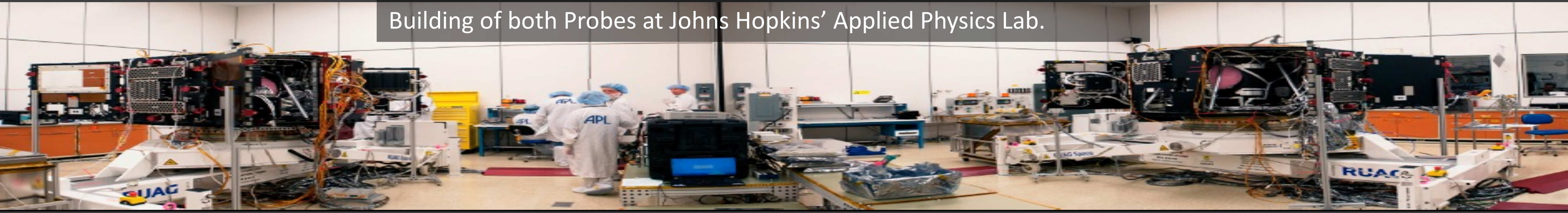

Building of both Probes at Johns Hopkins' Applied Physics Lab.

Two Recent Reviews on Radiation Belt Physics (2019-2020)

Particle Dynamics in the Earth's Radiation Belts: Review of Current Research and Open Questions

J.-F. Ripoll[1], S. G. Claudepierre[2,3], A. Y. Ukhorskiy[4], C. Colpitts[5], X. Li[6], J. F. Fennell[2], and C. Crabtree[7]

[1]CEA, DAM, DIF, Arpajon, France, [2]The Aerospace Corporation, El Segundo, CA, USA, [3]Department of Atmospheric and Oceanic Sciences, University of California, Los Angeles, CA, USA, [4]The Johns Hopkins University Applied Physics Laboratory, Laurel, MD, USA, [5]School of Physics and Astronomy, University of Minnesota, Minneapolis, MN, USA, [6]LASP, University of Colorado Boulder, Boulder, CO, USA, [7]Naval Research Laboratory, Washington, DC, USA

Citation:
Ripoll, J.-F., Claudepierre, S. G., Ukhorskiy, A. Y., Colpitts, C., Li, X., Fennell, J., & Crabtree, C. (2020). Particle Dynamics in the Earth's Radiation Belts: Review of Current Research and Open Questions. *Journal of Geophysical Research: Space Physics*, *125*, e2019JA026735. https://doi.org/10.1029/2019JA026735

- About 600 references
- Focus on major historical results and ultra recent studies from RBSP
- Focus on recent research and open questions
- But not a single image

Earth's Van Allen Radiation Belts: From Discovery to the Van Allen Probes Era

W. Li[1] and M.K. Hudson[2,3]

[1]Center for Space Physics, Boston University, Boston, MA, USA, [2]Department of Physics and Astronomy, Dartmouth College, Hanover, NH, USA, [3]High Altitude Observatory, NCAR, Boulder, CO, USA

Citation:
Li, W., & Hudson, M. K. (2019). Earth's Van Allen radiation belts: From discovery to the Van Allen Probes era. *Journal of Geophysical Research: Space Physics*, *124*, 8319–8351. https://doi.org/10.1029/2018JA025940

- About 350 references
- Well illustrated
- Enriched of figures from UCLA's and Dartmouth's groups studies

Motivation and objectives for radiation belt studies

Motivation:

Understand and compute the dynamics of the radiation belts

Objectives:

Synthetize all observations of electromagnetic waves and cold electron plasma density measured by the Van Allen Probes which drive wave-particle interactions (WPI) and RB dynamics

Generate formatted data & statistics usable for radiation belt physics

Perform accurate and validated radiation belt simulations

(Define best practices, lacks, and find ideas for new missions)

Objectives of this course:

Introduce whistler-mode hiss waves and focus on their fundamental role for radiation belt dynamics

Observation of the ambient environment: 1. the plasmasphere (briefly)

Available methods to deduce RBSP plasma density from wave instruments

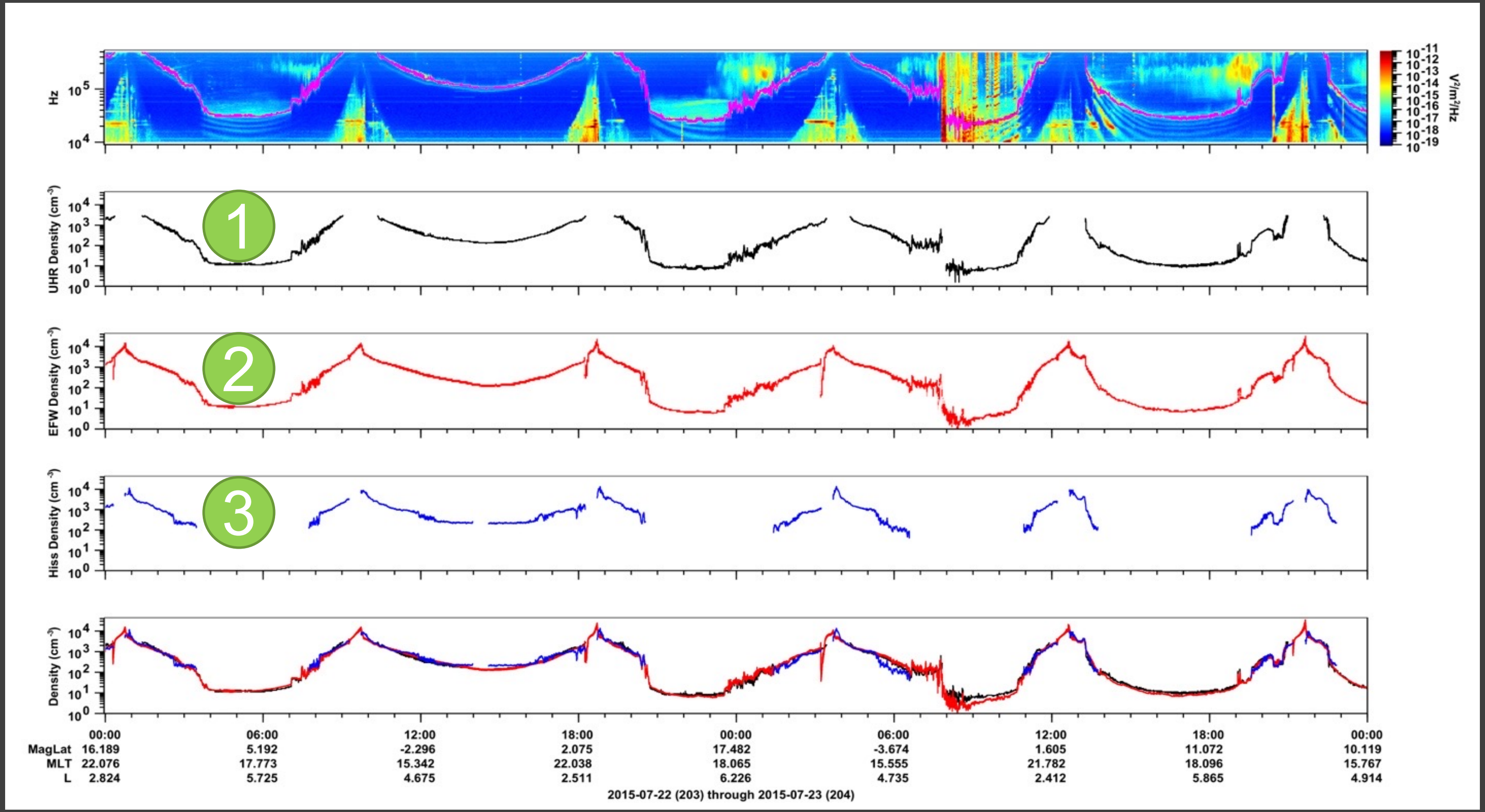

1

The upper hybrid resonance (UHR) method

$f_{pe}^2 = f_{UHR}^2 - f_{ce}^2$, (1) and $n_e = (f_{pe}/8980)^2$

(B. Kurth, D. Hartley and C. Kletzing)

Kurth+15

2

The s/c charging method from EFW (by S. Thaller)

$$n_e = n_{01} e^{-V_{sc}/V_1} + n_{02} e^{-V_{sc}/V_2}$$

Escoubet+97, Thaller+15, Jahns+20

3

Whistler inferred density: do (1) with your favorite (planar) whistler by D. Hartley. (2) Calibration phase with f_{UHR} (Hartley+18)

- Good agreement shown here between the 3 methods
- Next slides use method 2 calibrated with method 1 (see also Jahns+20 for comparisons)

The plasmasphere measured by s/c charging from RBSP during the whole mission

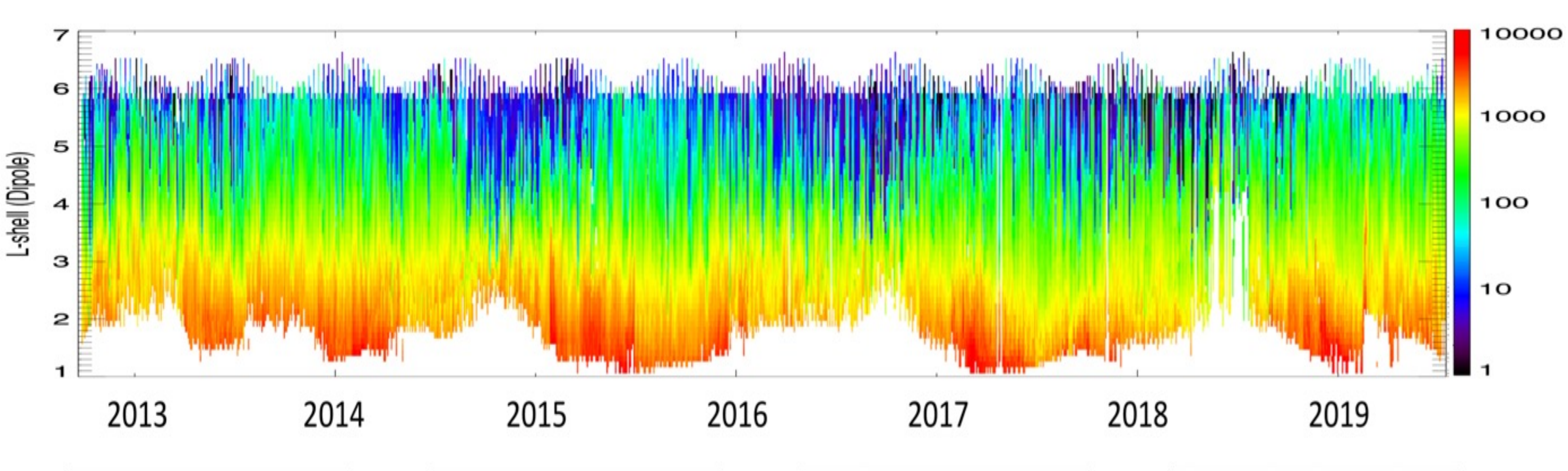

- S/c densities are most reliable within a range between ~10 cm^{-3} and 3000 cm^{-3}
- f_{uhl} density used for calibrating EFW S/c charging density at various dates (every ~ +/- 2-week interval of the days)
- RBSP orbit makes the analysis complex: low geomagnetic activity after 2016 not well visible.

Statistics of the plasmasphere s/c charging density sorted by Dst

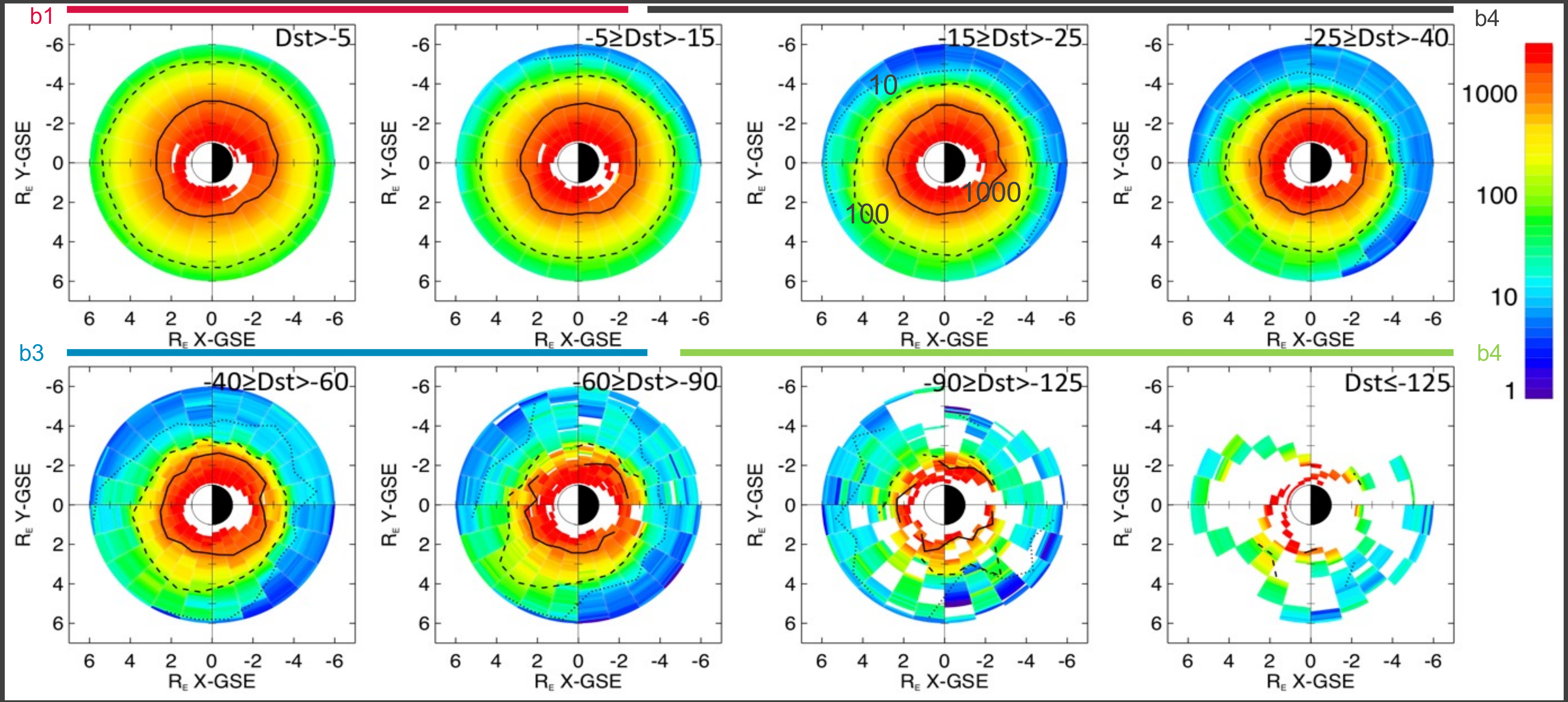

Ripoll et al., 2022 submitted

- Quiet times: isotropic plasmasphere extending above L=5 (almost L=6)
- Asymmetry forming with Dst increasing
- Plumes expanding further than L~6
- Detached plasma pockets wrapping around the Earth between L=4 and L=6
- Loosing resolution for Dst<-90
- The plasmapause position is a marker of activity
- No dynamic resolution of MLT with RBSP (MLT-dependence is only reached statistically)

- The outer electron belt lies within the plasmasphere for 40% of all times
- 65% of any RBSP data at a given L-shell falls within the plasmasphere, versus 35% in the plasma trough.

Geomagnetic activity during the Van Allen Probes

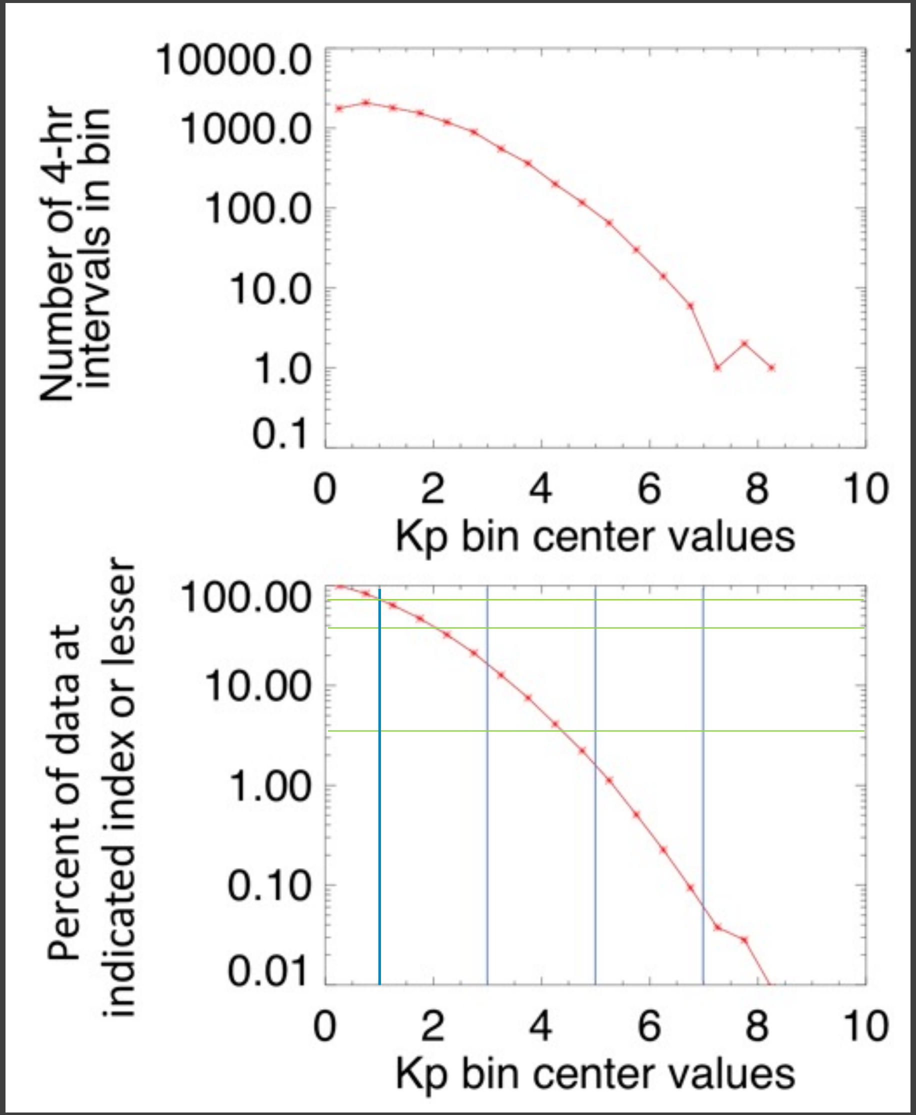

Kp <1 : 70% of RBSP coverage

Kp>3 : 10% of RBSP coverage

Kp>5 : 1% of RBSP coverage

Observation of the ambient environment: 2. whistler-mode waves

The whistler wave picture from Summers et al. 1998

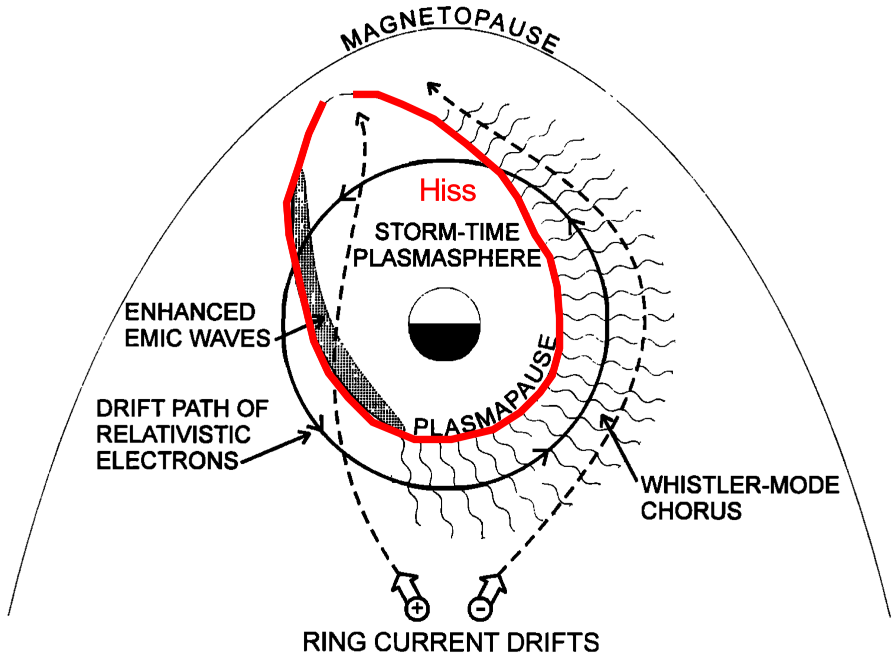

Figure 7. Schematic diagram showing spatial distribution of whistler mode chorus and EMIC waves during magnetic storms in relation to the position of the plasmapause and the drift paths of ring current (10–100 keV) electrons and ions and relativistic ($\gtrsim$ 1 MeV) electrons.

More recent versions of this map are in

- Thorne, R. M. (2010), Radiation belt dynamics: The importance of wave-particle interactions, Geophys. Res. Lett., 37, L22107, doi:10.1029/2010GL044990.
- Kletzing, C. A., Kurth, W. S., Acuna, M., MacDowall, R. J., Torbert, R. B., Averkamp, T., et al. (2013). The Electric and Magnetic Field Instrument Suite and Integrated Science (EMFISIS) on RBSP. Space Sci. Rev. 179 (1-4), 127–181. doi:10.1007/s11214-013-9993-6
- Reeves, G. D., et al. (2016), Energy- dependent dynamics of keV to MeV electrons in the inner zone, outer zone, and slot regions, J. Geophys. Res. Space Physics, 121, 397–412, doi:10.1002/ 2015JA021569.
- Li, W., & Hudson, M. K. (2019). Earth's Van Allen radiation belts: From discovery to the Van Allen Probes era. Journal of Geophysical Research: Space Physics, 124, 8319–8351. https://doi. org/10.1029/2018JA025940

But there is a more complex MLT dependence we'll address later

Whistler-mode waves zoo observed dynamically from space:

Plasma density

Power Spectral Density (PSD)

Macroscale Stucture

Power Spectral Density

Microscale Structure

Courtesy D. Malaspina

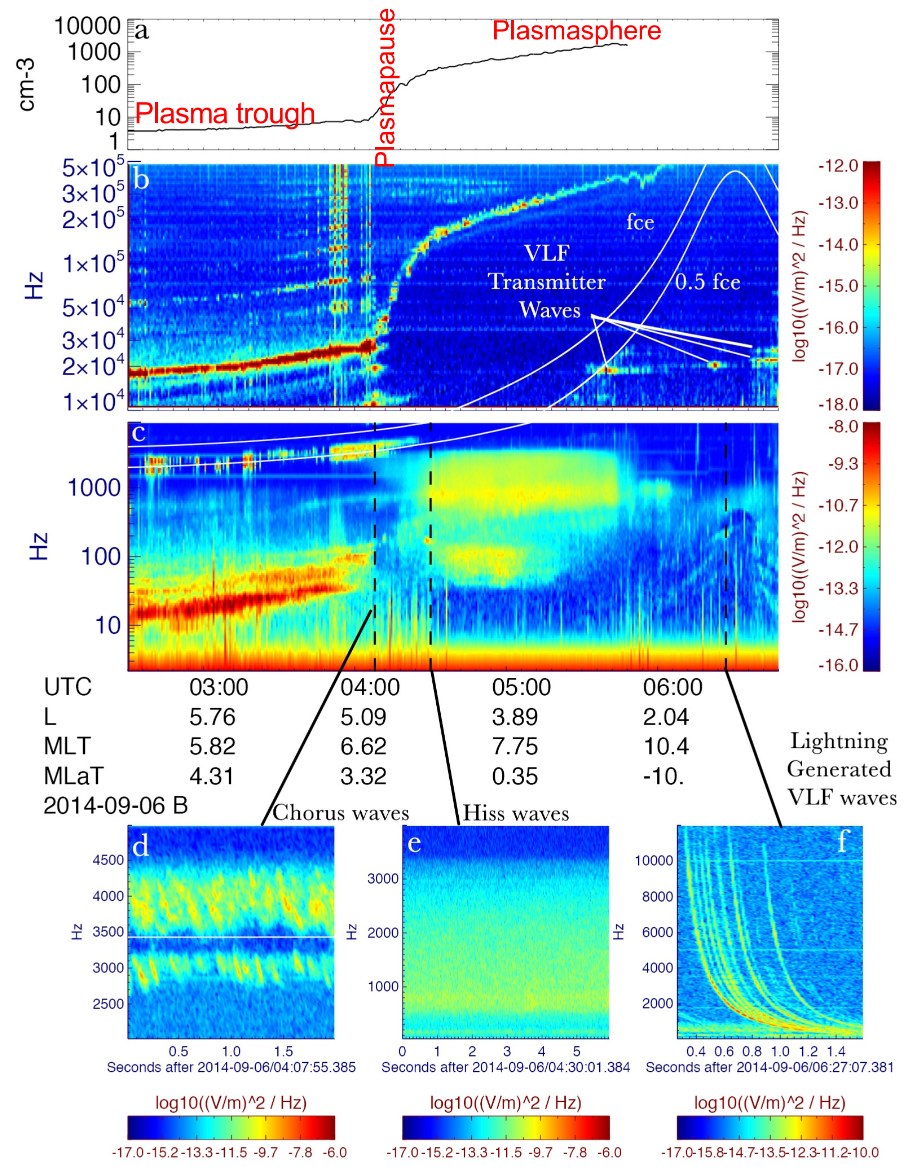

Most prominent waves:

- Plasmasphere with whistler mode hiss waves
- Chorus waves in the plasma trough

Less prominent waves:

- VLF Transmitter waves
- Lightning-generated whistler-waves (LGW)

The max EM power of EM waves:

- Hiss : RMS(B)=16 pT in 10-14 MLT for 300-650 Hz from Polar satellite (Falkowski+17)
  RMS(B)=38 pT all storms measured by the Van Allen Probes between 9/ 2012 and 12/2018 (Malaspina+18)
  Max ~200 pT for extreme hiss in plumes (Shi+19, Millan & Ripoll 21)
- Lightning superbolt whistlers: RMS(B)~83 pT
- Chorus max. ~ 3 nT (Hospodarsky+16)
- EMICs max ~ 10 nT (Engebretson+2015)
- Whistler-mode waves (non-LGW) : RMS(E)~250 mV/m (Cattel+08)

Whistler-mode hiss waves : generalities. (1/3)

- Whistler mode hiss waves leave in the plasmasphere (Thorne et al., 1973)
- Frequencies from ~50 Hz to ~2 kHz from L ~ 2 up to the plasmapause
- Right hand polarized with ellipticity above ~0.2 up to ellipticity >0.5 and polarization >0.5
- Widely regarded as broadband, structureless, incoherent emission waves
- Hiss waves occur for any geomagnetic activity
- MLT-dependent model of hiss (RBSP) in Spasojevic et al. (2015)

- Higher-frequency hiss (2–10 kHz) have also been reported.

- Exception: Summers et al. (2014) showed evidence that plasmaspheric hiss could be a coherent emission with fine structure. Some coherence also observed with polar in plumes (solar min. conditions, Tsurutani et al., 2015)

- Whistler mode hiss waves are also observed in high-density plumes outside the plasmasphere and with ongoing characterization of their properties

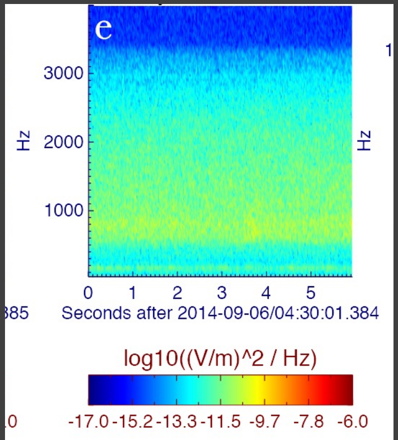

Main references

Li+, 2015
Meredith+, 2004, 2006
Tsurutani+, 2015
Kim+, 2015
Spasojevic+ 2015
Malaspina+ 2016, 2018
Meredith+ 2018
Hartley+2018

He+ 2019
Chan & Holzer, 1976;
Summers+ 2008

Woodroffe+ 2017
Su+ 2018
Shi+ 2019
Li+ 2019
Zhang+, 2018, 2019
Millan+, 2021

Whistler-mode hiss waves : the open debate on their origins. (2/3)

Open debate for decades : origins from chorus (?)

- Bortnik, Thorne, and Meredith (2008) : plasmaspheric hiss originates from chorus emissions, which are generated outside the plasmasphere. Chorus would propagate into the plasmasphere where they become trapped. Ray tracing studies support this scenario.
- This thesis is also supported by global statistical evidence based on chorus waves measurements from 6 different satellites (Meredith, Horne, Glauert, et al., 2013).
- Simultaneous appearance and disappearance of hiss and chorus waves could support this theory (Liu et al., 2017).

BUT

- Hartley et al. (2019) used Van Allen Probes observations coupled to ray tracing simulation and found a spatial limitation of the wave vector orientation indicating that chorus waves may only contribute to a small fraction of the plasmaspheric hiss wave power.
- Internal generation is a plausible alternative. Falkowski et al. (2017) suggest midnight injections of energetic electrons from substorm or small injection event (nonstorm events) could generate hiss.
- Nonlinear mechanisms of generation and growth of hiss may help to reveal their origin

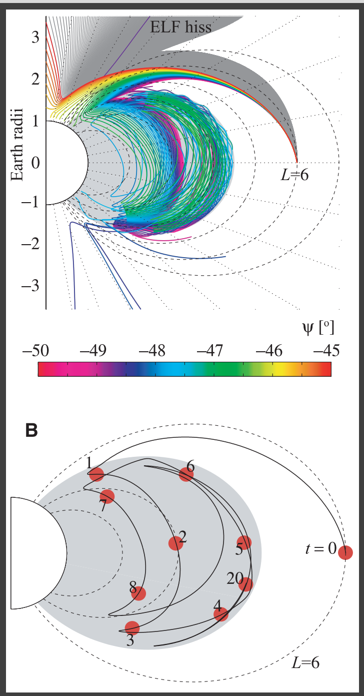

Bortnik, Science, 2009

Main references:

Chen+, 2012a, 2012b
Chen+, 2012b, 2012c

Omura, Nakamura, et al., 2015
Nakamura+, 2016

Whistler-mode hiss waves : known as a powerful scattering wave. (3/3)

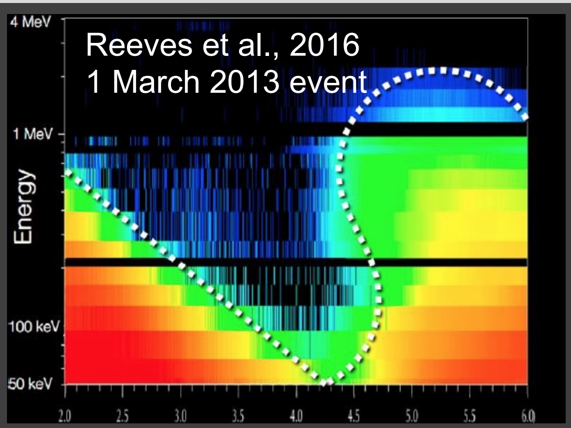

- Lyons & Thorne, 1973: Whistler mode hiss waves are the main driver of the slot formation and the well-known, energy dependent, two-belt structure of the radiation belts
- Hiss power can be locally high (>50^2 pT2), but their important effects come from their sustained power (often ~10^2 pT2) in a vast domain (L > ~2 up to the plasmapause location).
- Breneman et al., Nature, 2015 : strong visible coherence between the hiss amplitude (1 to 4 days after a storm) and electron loss observed in the form of bremsstrahlung X-rays measured from a BARREL balloons flying at altitudes of ~35 km over Antarctica, with modulations correlated with the variation of the plasma density and the magnetic field
- Due to their great contribution to particle scattering, the statistical distribution of hiss wave properties needs to be well characterized in magnetic local time (MLT), L-shell, and geomagnetic activity.
- Numerous studies have been devoted to hiss-driven loss.

References:

Meredith+, 2006
Li, Ni, et al., 2014;
Ni+, 2013, 2014, 2017;
Orlova+, 2014;
Hardman+, 2015;
Gao+, 2015;
Hua+, 2019;
Li+, 2019;
Reeves+, 2016;
Ripoll+, 2016,2017, 2019, 2020

Whistler-mode Waves and Plasma Density for WPI

WPI = wave particle interactions

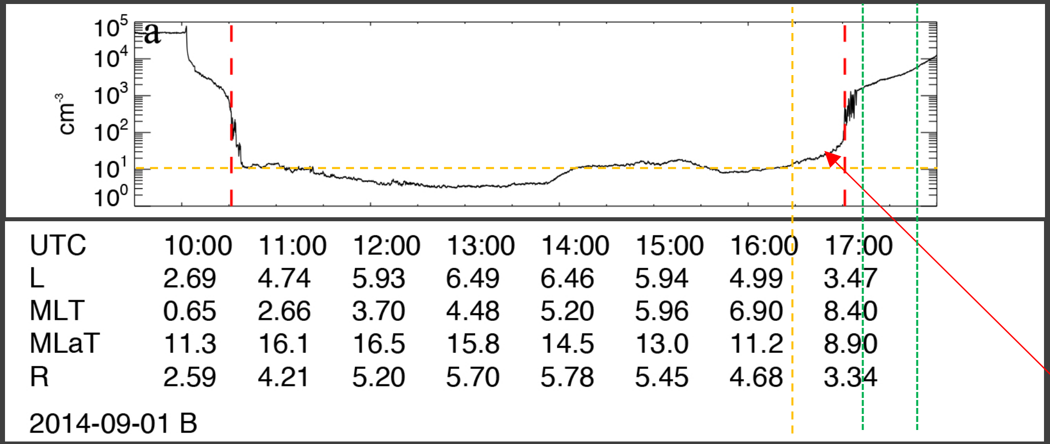

The plasmapause is a dynamic boundary in both space and time with respect to L-shell.

Complexity arises inside the plasmapause (150-10 #/cc), in plasma plumes and in detached plasma (also in very dense low-L regions)

Whistler-mode Waves and Plasma Density for WPI

WPI = wave particle interactions

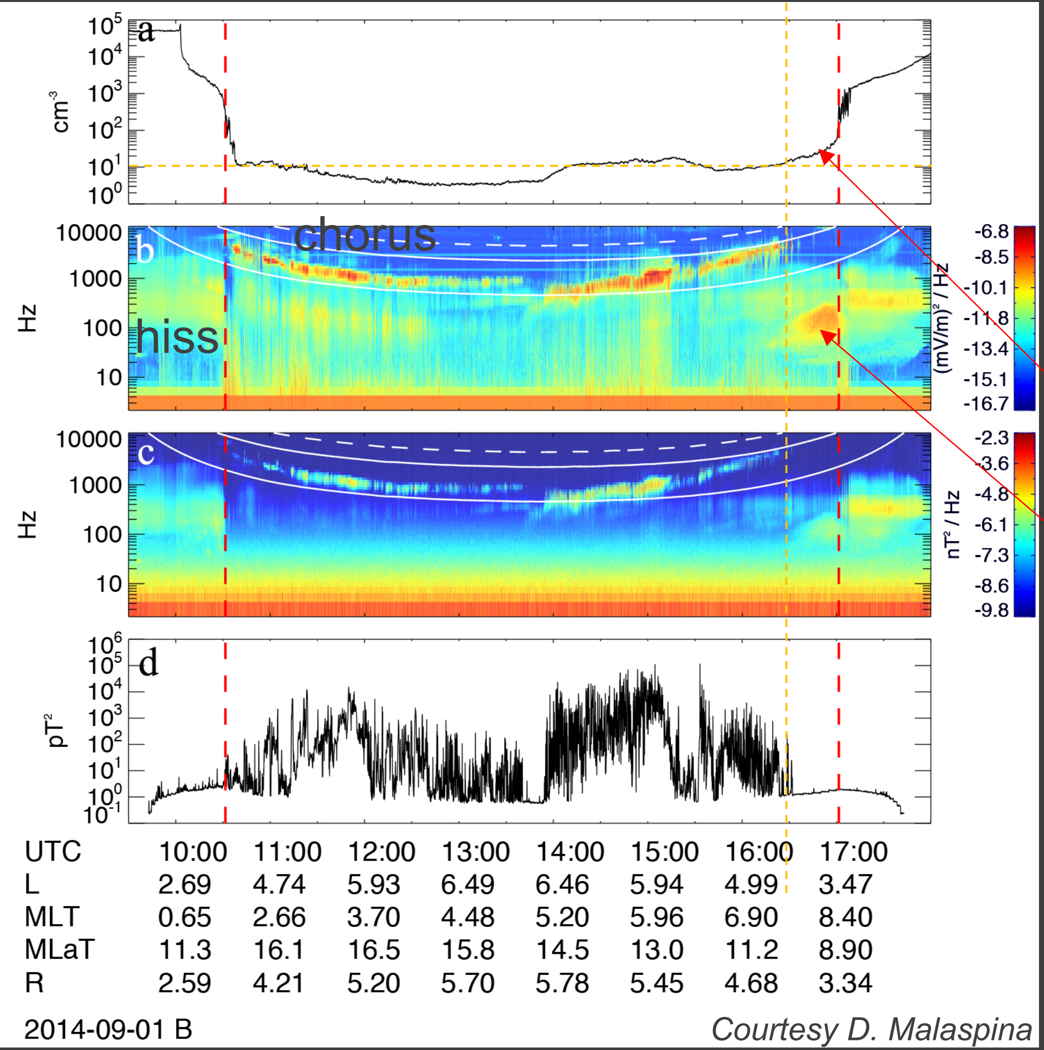

The plasmapause is a dynamic boundary in both space and time with respect to L-shell.

Complexity arises inside the plasmapause (150-10 #/cc), in plasma plumes and in detached plasma

In these regions live low-frequency hiss waves

Whistler waves can be a good marker of the plasmasphere boundary layer

Knowing both wave & plasma condition simultaneously is capital for good WPI computation

High Correlation between Plasmaspheric Hiss Wave Power and Plasma Density

Hiss Power Sorted vs L

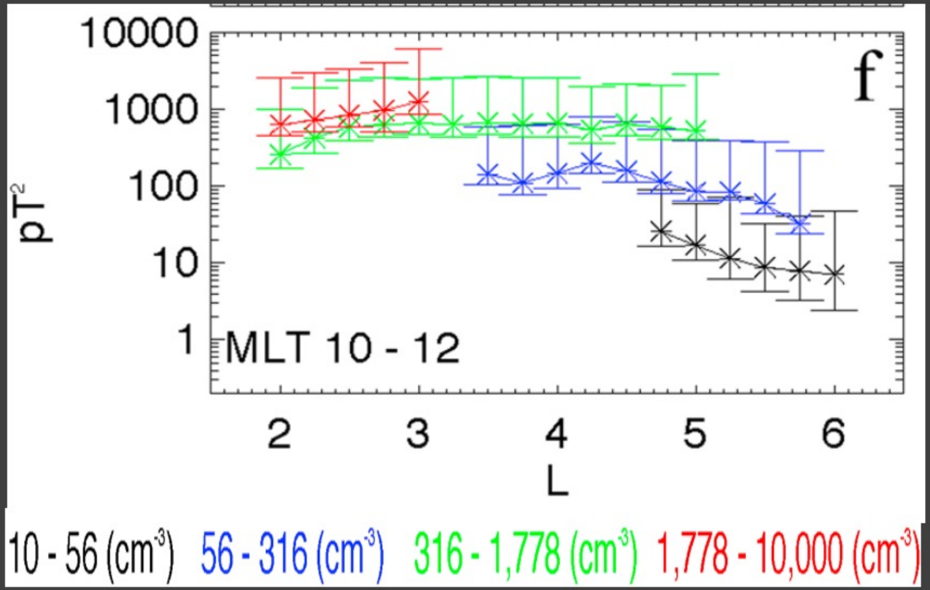

→ Hiss sorted with plasmapause location in Malaspina et al. GRL 2017

→ New sorting with density

New Hiss Power Sorted vs Density

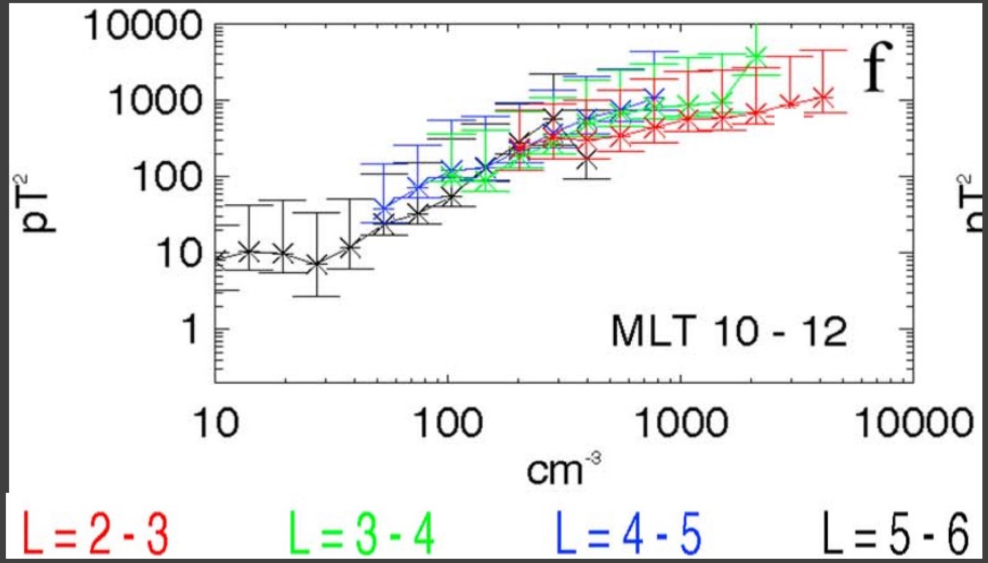

Plasmaspheric hiss wave power strictly increases with plasma density (L>~2.5*)

- This increase is stronger and occurs regardless of L and for all MLTs (L>~3)
- These conclusions hold for variable AE*
- This correlation pleads in favor of a local generation mechanism for hiss (open subject cf. review Rad. Belt Physics, Ripoll et al. JGR 2020)

Malaspina, D. M., Ripoll, J.-F., Chu, X., Hospodarsky, G., Wygant, J. (2018). Variation in plasmaspheric hiss wave power with plasma density. Geophysical Research Letters, 45. https://doi.org/10.1029/2018GL078564

No apparent link between chorus waves and plasmapause position

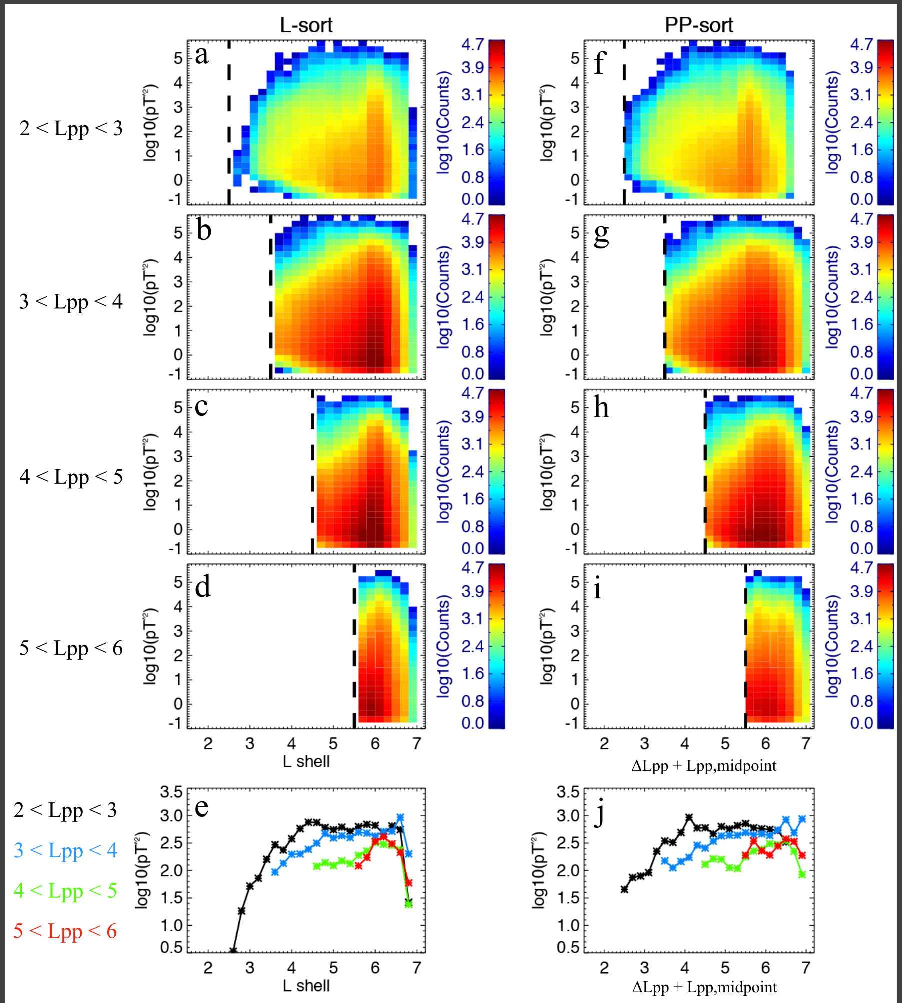

Maiaspina, et al. Testing the Organization of Whistler-mode Chorus Wave Properties by Plasmapause Location Journal of Geophysical Research, 2021

Statistics computed for 7 years of Van Allen Probes data

No particular link between the plasma density and the chorus

→ No sorting with Lpp

→ Certainly L> Lpp defines the chorus region

→Still some ongoing work

Plasmasphere and whistler-mode waves coupled response to mild substorms injections

Ripoll et al. 2020, JASTP

Plasma density data: from EMFISIS (Kurth et al.) and SCC from EFW (S. Thaller, LASP)

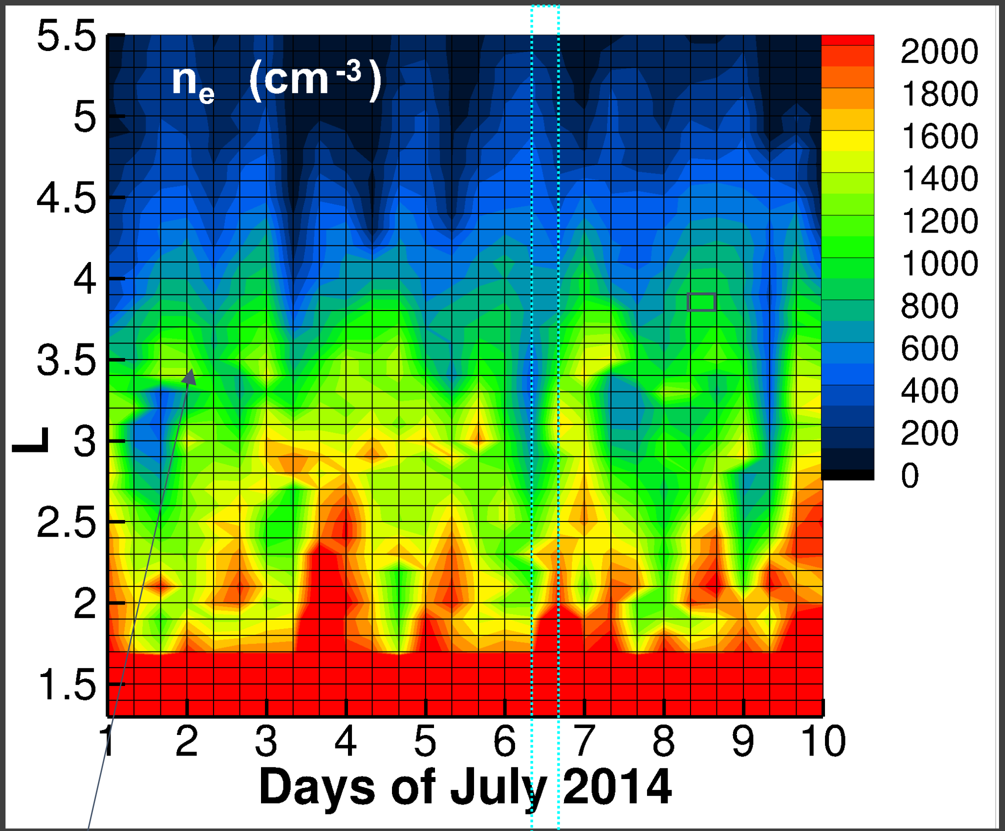

One cell of the observation/simulation

Time bin = Av. of Ne during 8 hours (~1 RBSP path) within 0.1L

Mean Hiss Frequency

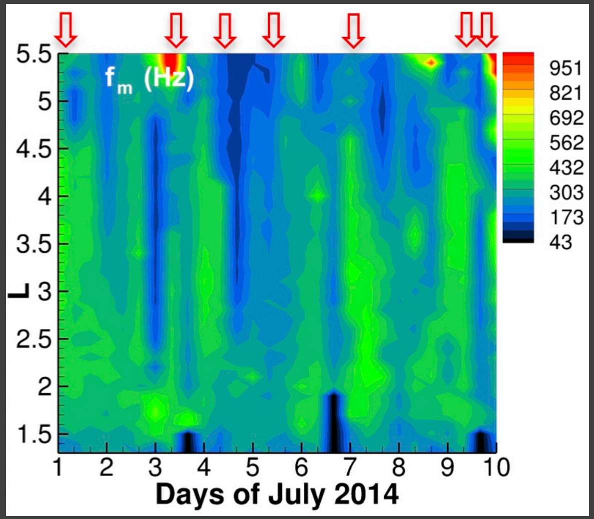

Hiss power

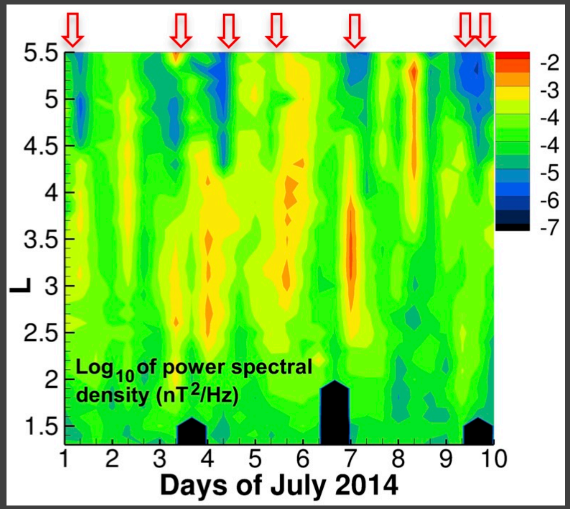

- 3 frequency populations, two for hiss (200–400 and 600–800 Hz), and chorus can be in the 1-2 kHz hiss band outside the plasmasphere
- Wave amplitudes vary by orders of magnitude.
- Hiss power confined inward during injections
- The stronger hiss waves are located in the plasmasphere interior, between L = 2 and L = 4.
- Wna response not shown

Antagonist effects

- Density decreases →favors scattering
- But wave power decreases →does not favor scattering

The whistler-mode statistical wave zoo system (L-shell sorted)

Extension of Malaspina et al. GRL 2017 to the whole RBSP mission: the whistler zoo

Work in progress

High activity (Lpp=2-3, MLT=noon) Low activity (Lpp=5-6, MLT=noon)

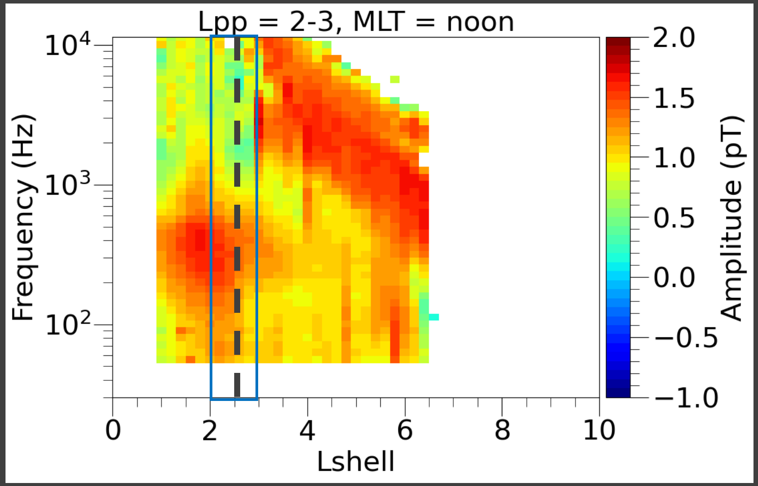

- Overlap of hiss/chorus in L~2-3 and L~5-6

(Ripoll, Malaspina, Cunningham, Cosmides et al. 2022, in preparation)

Extension of Malaspina et al. GRL 2017 to the whole RBSP mission: the whistler zoo

Work in progress

High activity (Lpp=2-3, MLT=noon)

Low activity (Lpp=5-6, MLT=noon)

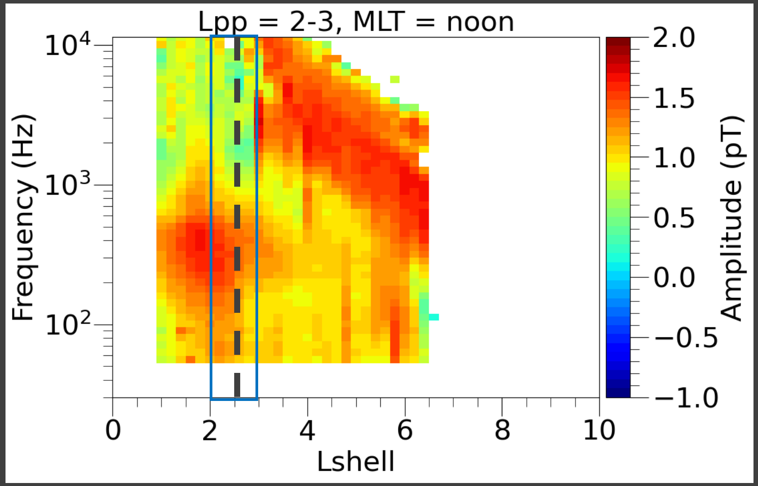

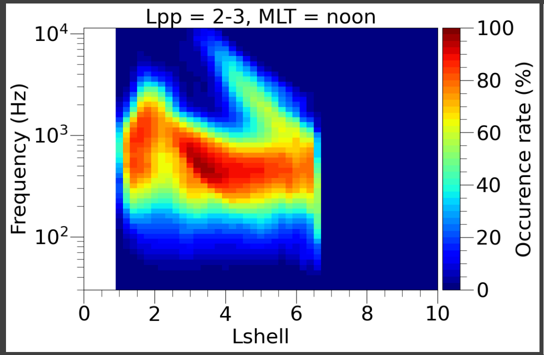

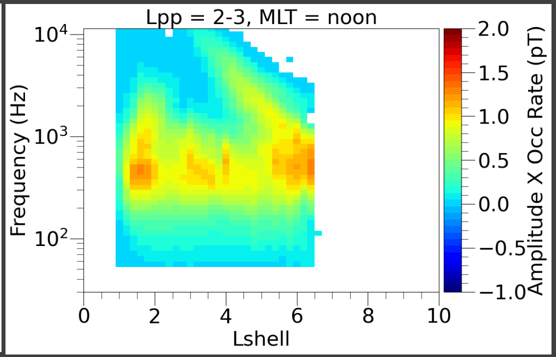

- Overlap of hiss/chorus in L~2-3 and L~5-6
- Importance of hiss up to L~6 (plume effects in stats)

(Ripoll, Malaspina, Cunningham, Cosmides et al. 2022, in preparation)

The whistler-mode statistical wave zoo system (L-shell sorted)

Extension of Malaspina et al. GRL 2017 to the whole RBSP mission: the whistler zoo

Work in progress

High activity (Lpp=2-3, MLT=noon)

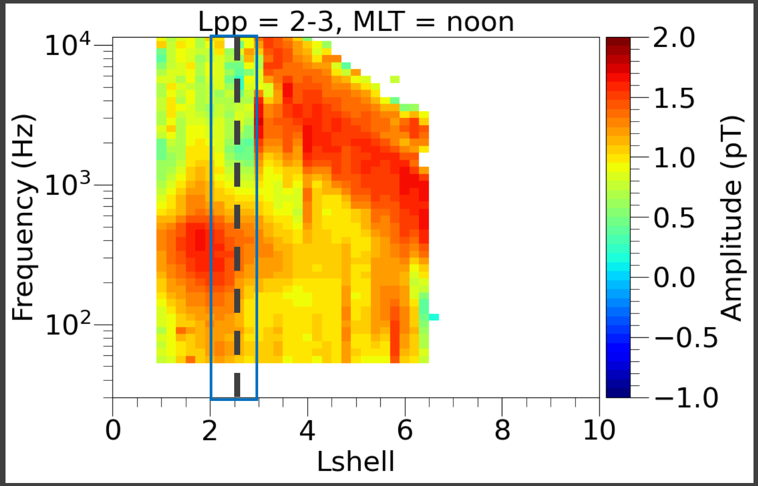

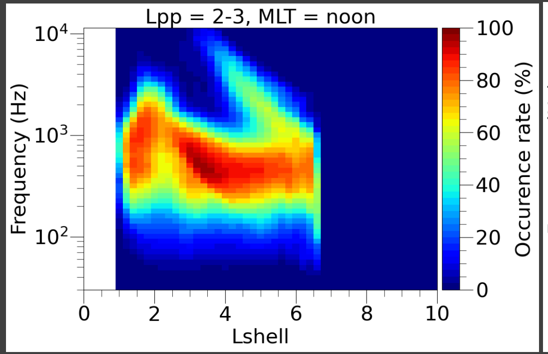

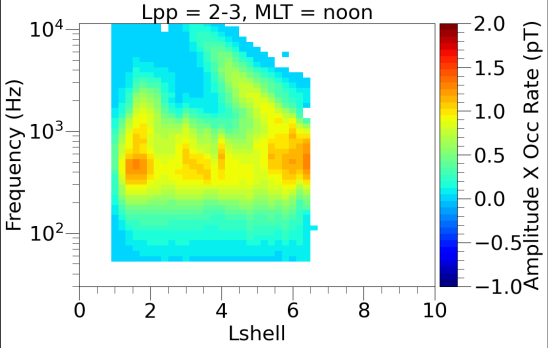

- Overlap of hiss/chorus in L~2-3 and L~5-6
- Importance of hiss up to L~6 for quiet times

Low activity (Lpp=5-6, MLT=noon)

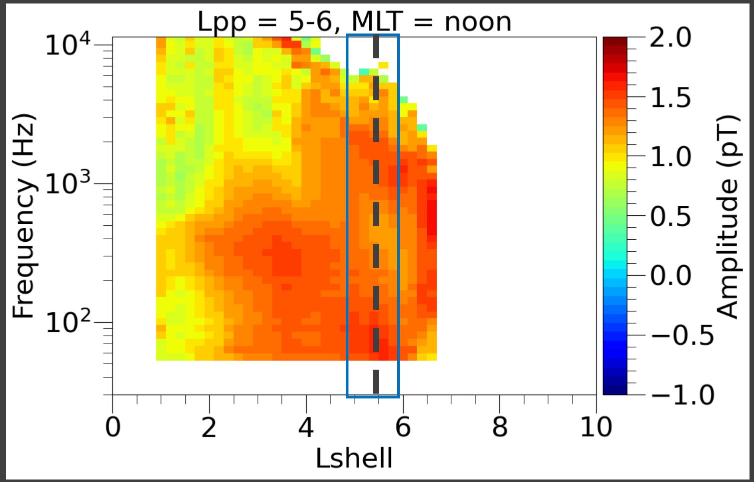

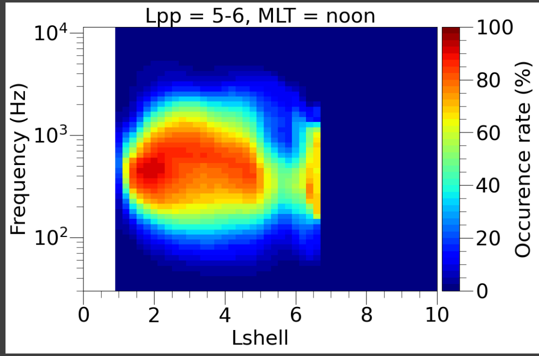

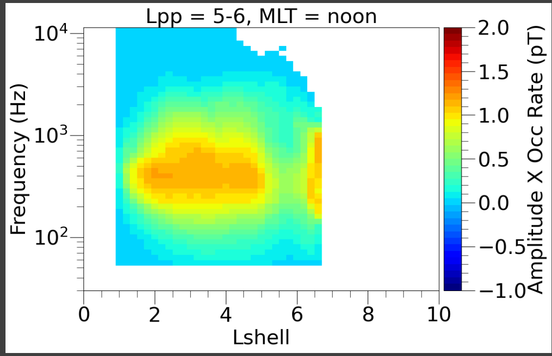

- Importance of plasmasphere and wave coupling
- The statistical approach mixes the effects

(Ripoll, Malaspina, Cunningham, Cosmides et al. 2022, in preparation)

Mean power and mean frequency of hiss and chorus waves

Work in progress

MLT=dawn

MLT=noon

Power

Mean frequency

Active Lpp=2-3

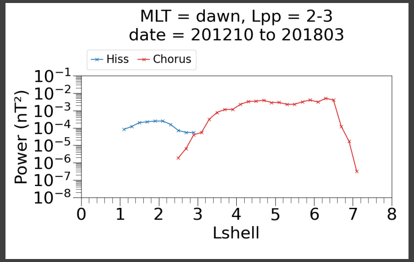

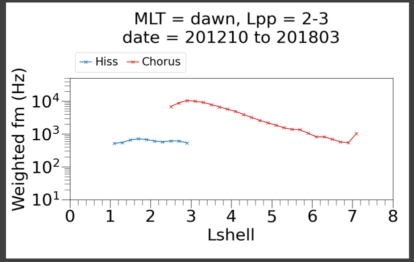

Power

Mean frequency

Active Lpp=2-3

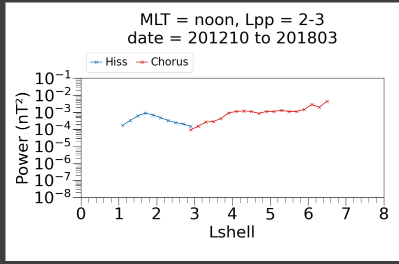

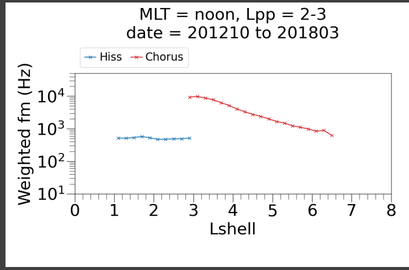

- No occurrence rate factored (yet)
- Would be used for statistical simulations (not done here)

(Ripoll, Malaspina, Cunningham, Cosmides et al. 2022, in preparation)

Mean power and mean frequency of hiss and chorus waves

Work in progress

MLT=dawn

Power / Mean frequency

Active Lpp=2-3

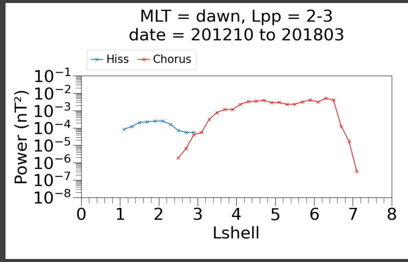

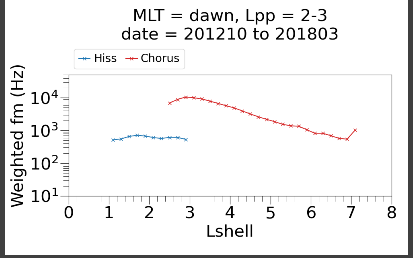

Quiet Lpp=5-6

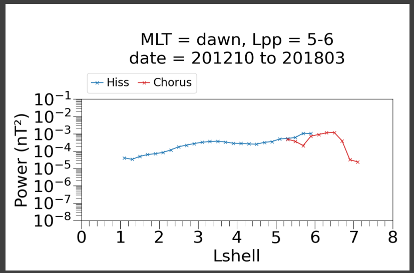

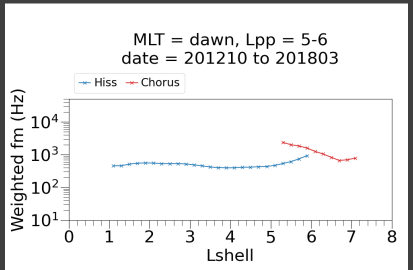

MLT=noon

Power / Mean frequency

Active Lpp=2-3

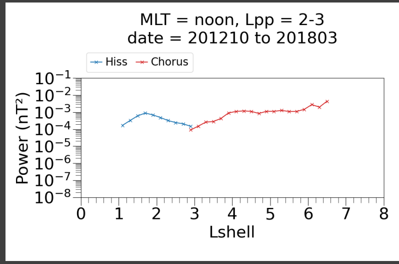

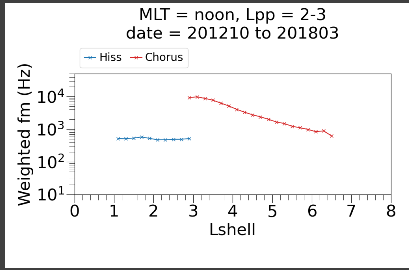

Quiet Lpp=5-6

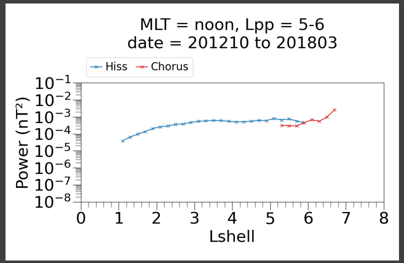

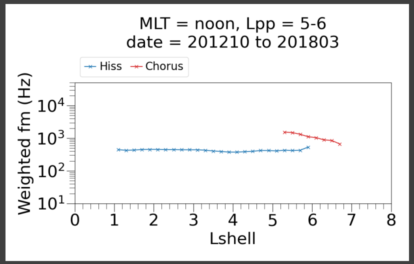

Would be used for statistical simulations (not done here)

(Ripoll, Malaspina, Cunningham, Cosmides et al. 2022, in preparation)

Hiss waves in plasmaspheric plumes : revealed as intense by RBSP

- RBSP-B enters plasmaspheric plume, followed by RBSP-A (2 orbits)
- Intense hiss observed in the the plume

EMFISIS observations of wave power

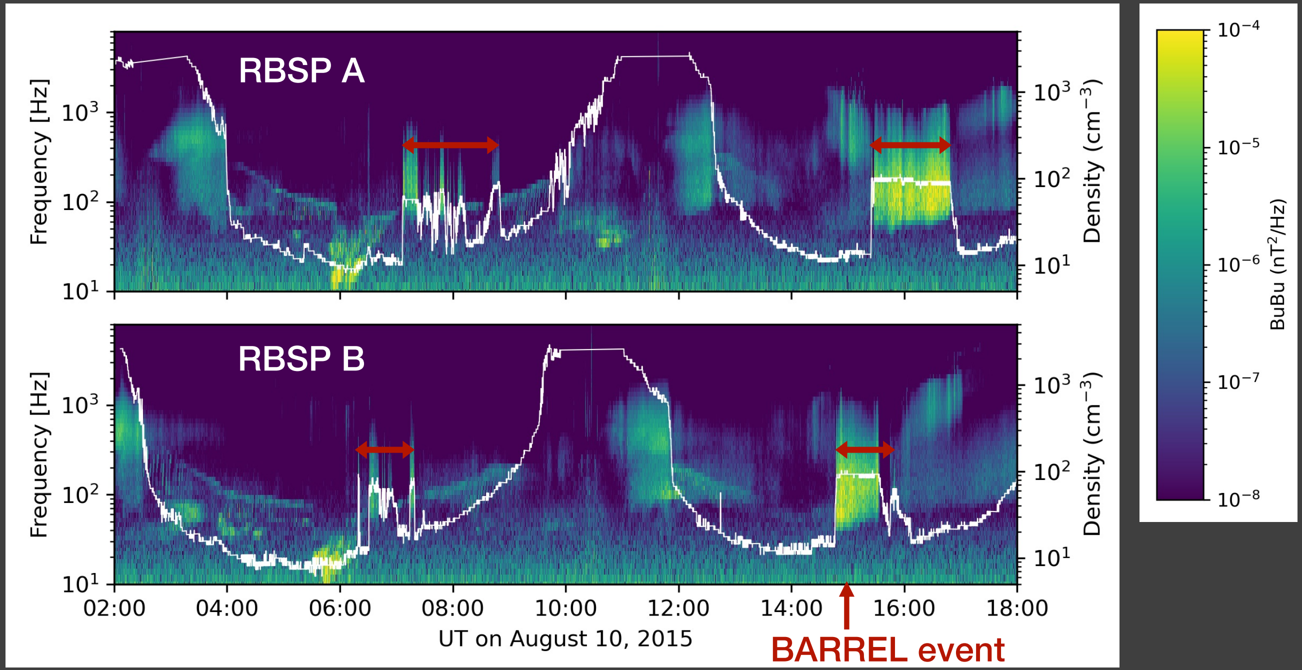

Local plasma and wave properties

Spacecraft RBSP	Time UT	Amplitude (pT)	f_{median} (Hz)	f_{min} (Hz)	f_{max} (Hz)	θ (degrees)
A	1500–1700	140	154	76	313	11
B	1440–1540	92	150	63	400	12

Spacecraft RBSP	n_e (cm^{-3})	ω_{pe} $\times 10^5 s^{-1}$	ω_{ce} $\times 10^3 s^{-1}$	ω_{med}/ω_{ce} $\times 10^{-1}$	$\omega_{med}\omega_{ce}/\omega_{pe}^2$ $\times 10^{-5}$
A	79.4	5.03	4.26	0.97	1.63
B	79.4	5.03	4.26	0.94	1.59

Millan et al. 2021

Observations of the radiation belts from Van Allen Probes

Van Allen Probes Observations of the radiation belts

Reeves et al. 2016

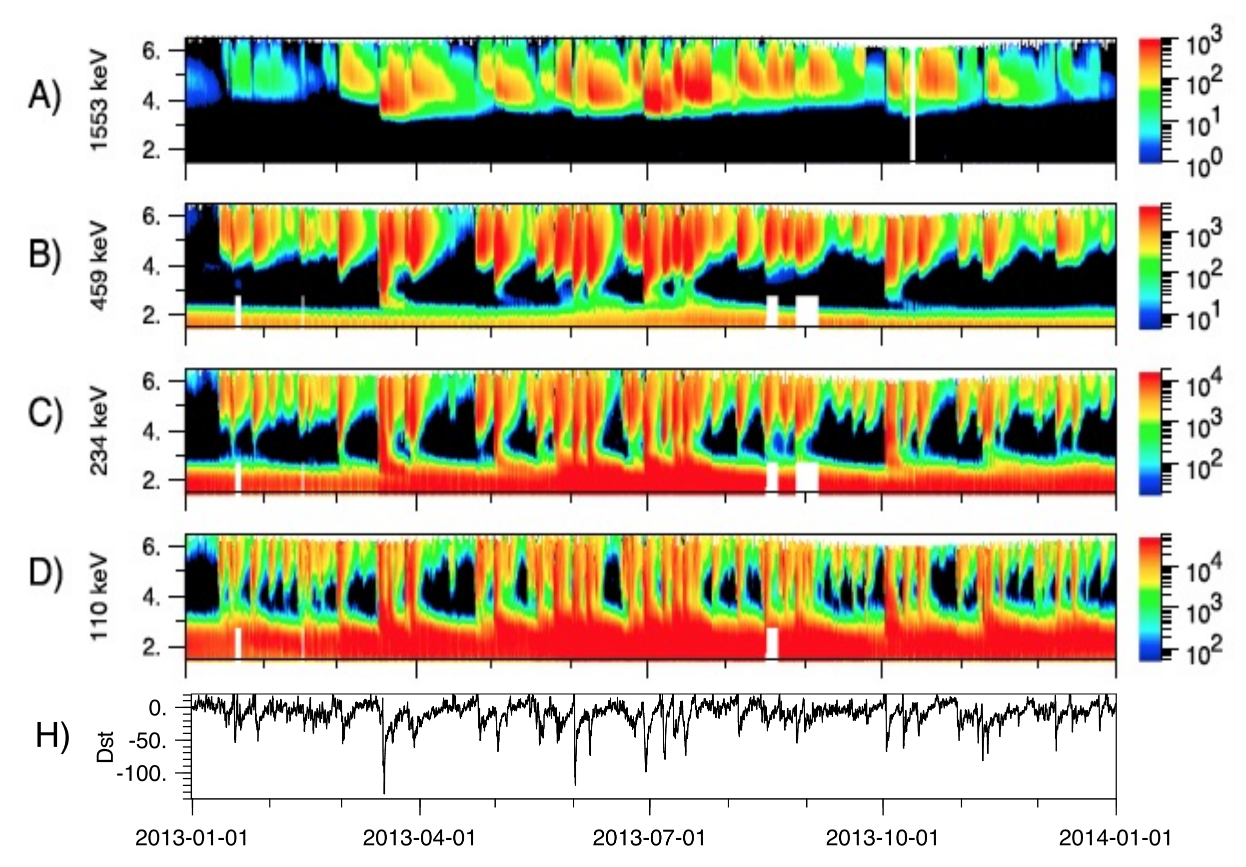

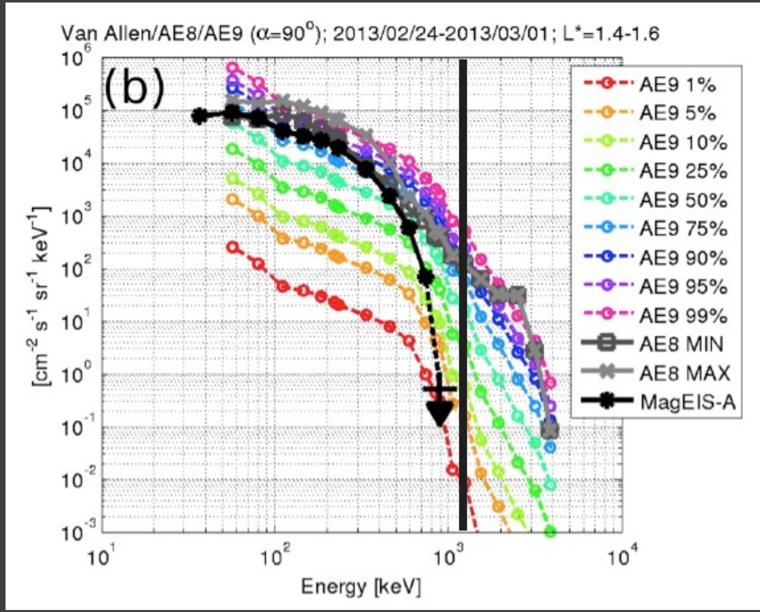

Van Allen Probes show the inner radiation zone contains no MeV electrons by Fennell et al., GRL, 2015)
The impenetrable barrier, Baker et al., *Nature* [2014]

- Storm and substorm injections (~250 keV Turner et al. 2015)
- Clear energy dependence of the location of the belt
- Discovery of Fennell's 2015 limit of the Inner RB at ~1 MeV
- E-structure discuss throughout the talk

Ripoll, J.-F., Claudepierre, S. G., Ukhorskiy, A. Y., Colpitts, C., Li, X., Fennell, J., & Crabtree, C. (2020). *Particle Dynamics in the Earth's Radiation Belts: Review of Current Research and Open Questions*. Journal of Geophysical Research: Space Physics, 125, e2019JA026735.

Pitch angle dependence of the outer belt (Oct. 2013)

RBSP MagEIS data

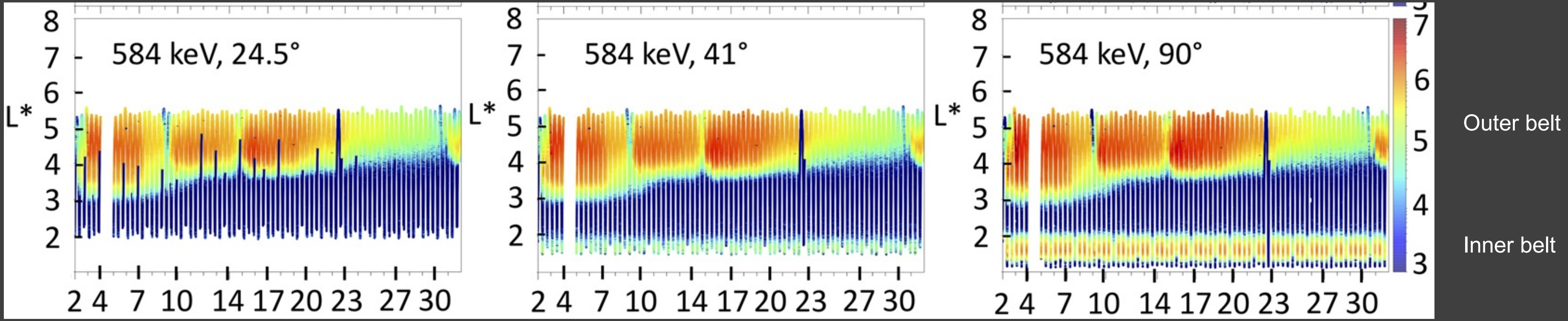

From Pierrard, V., Ripoll, et al., JGR 2021

- Flux intensification as pitch angle increases
- No change in the inner boundary of the outer belt as pitch angle changes
- Weak dependence in p.a. of the outer radiation belt
- Strong dependence in p.a. of the inner radiation belt
- Dependence will be quantified/explained with simulations

High energy injection in the inner belt in October 2013 : strong p.a. dependence

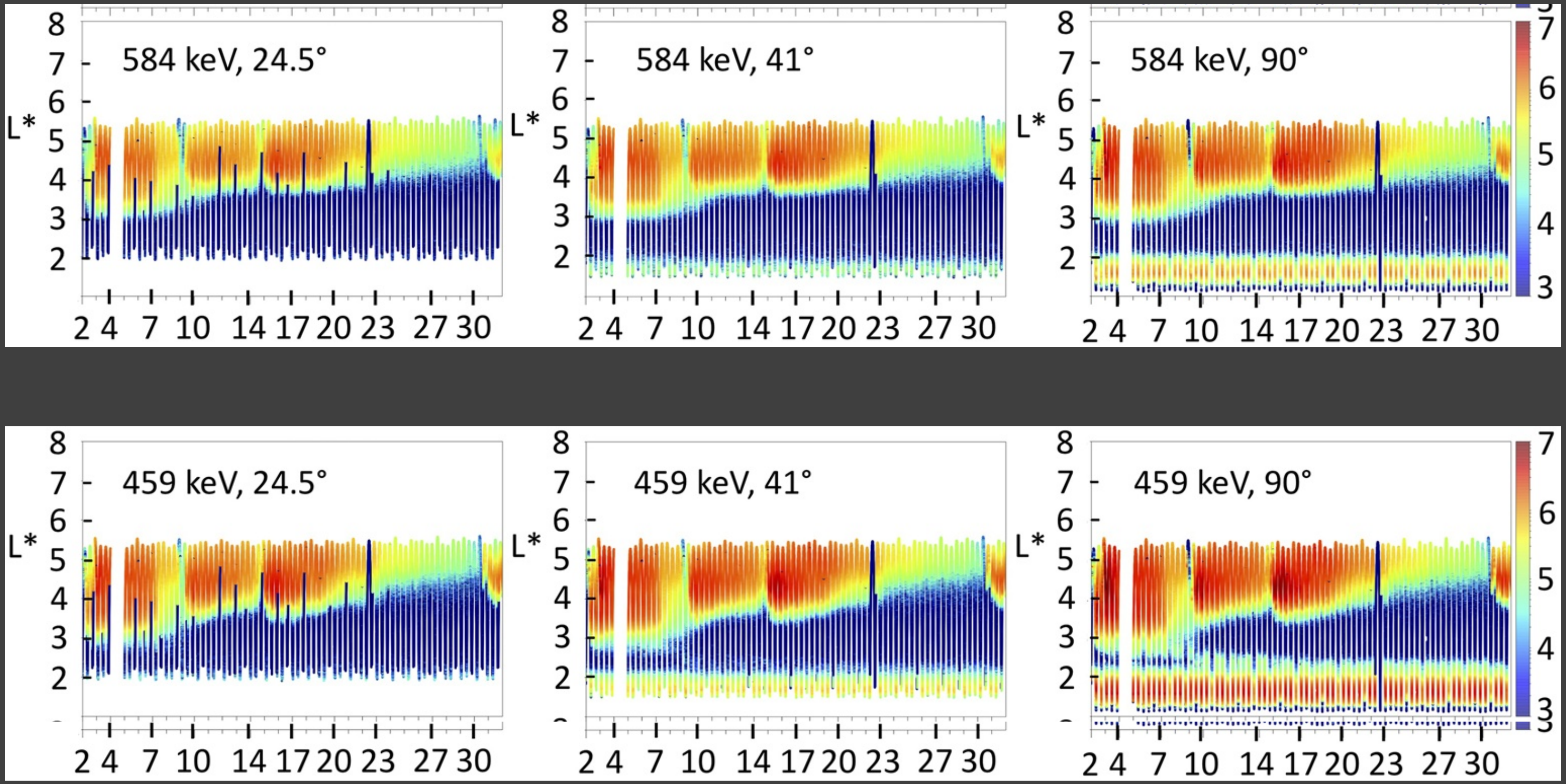

Injection absent at 584 keV

Injection visible at 459 keV and high pitch angle only

From Pierrard, V., Ripoll, et al., 2021

- A high energy injection penetrates the inner belt on October 2.
- Injection observed at 459 keV and absent in the next channel
- Common substorm electron injections is ~250 keV (e.g. Turner et al., 2015).

Comparing GTO and LEO radiation belt flux in October 2013

RBSP: GTO

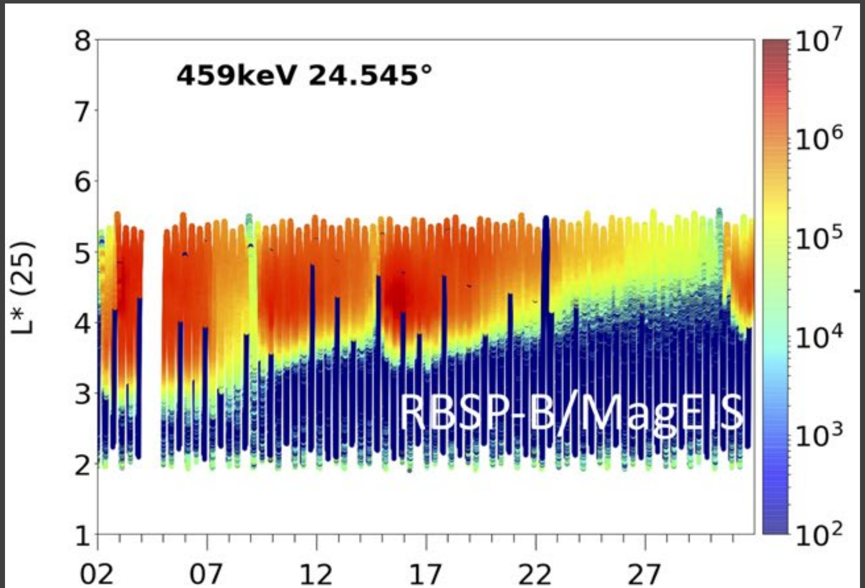

Proba V: LEO

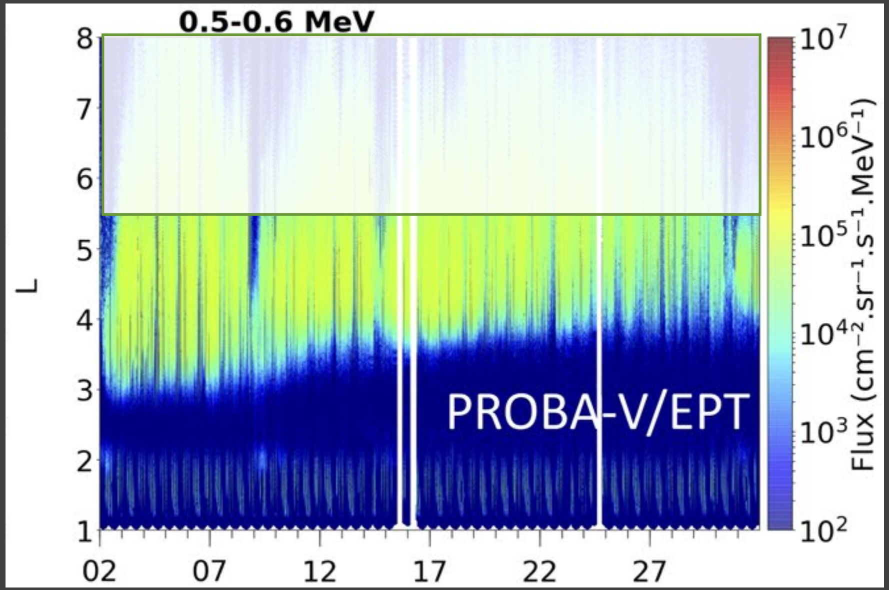

- Good overlap of the ORB observed at LEO (low p.a., high lat.) and by RBSP (low p.a., lat.<20°)
- Changing $L_{<25}$ by L^*_{25} affects the upper edge of the outer belt by ~1 L in spreading the outer belt to higher L-shells, but does not change the lower L-shell limit.
- Concordance of the dropouts
- The EPT flux is lower than the RBSP flux. (Possible reasons : 24° is already likely too high in pitch angle to match the Proba V/EPT flux. MagEIS aperture and time integration. Lower energy range for RBSP, leading to higher fluxes. No inter-calibration yet available)

Pierrard, V., Ripoll, J.-F., Cunningham, G., Botek, E., Santolik, O., Thaller, S., et al. (2021). Observations and simulations of dropout events and flux decays in October 2013: Comparing MEO equatorial with LEO polar orbit. *Journal of Geophysical Research: Space Physics*, *126*, e2020JA028850. https:// doi.org/10.1029/2020JA028850

The equilibrium structure a good illustration of hiss wave scattering effects that sculpt the belts structure during quiet times

1

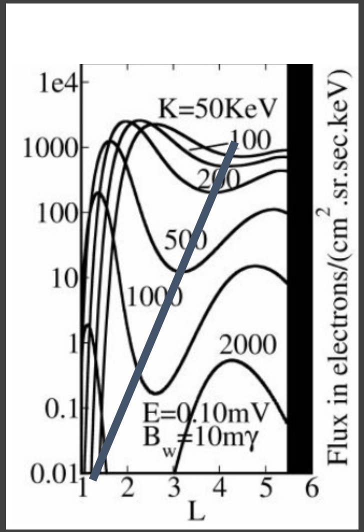

Lyons and Thorne, 1973

Made of RD=HL

The E-structure of the belts is energy dependent

2

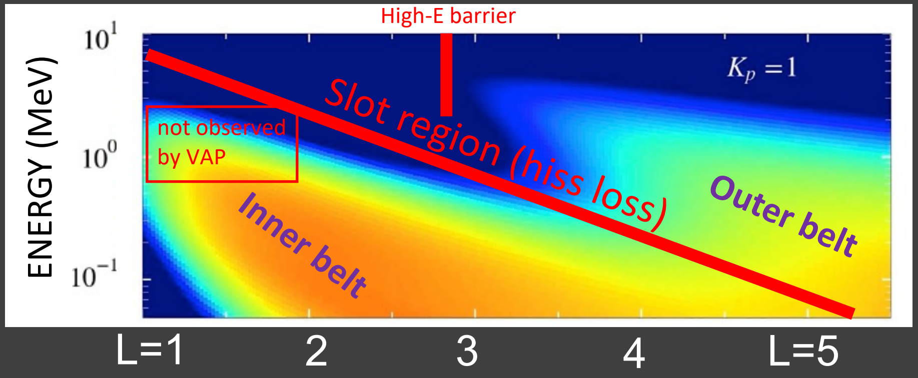

3

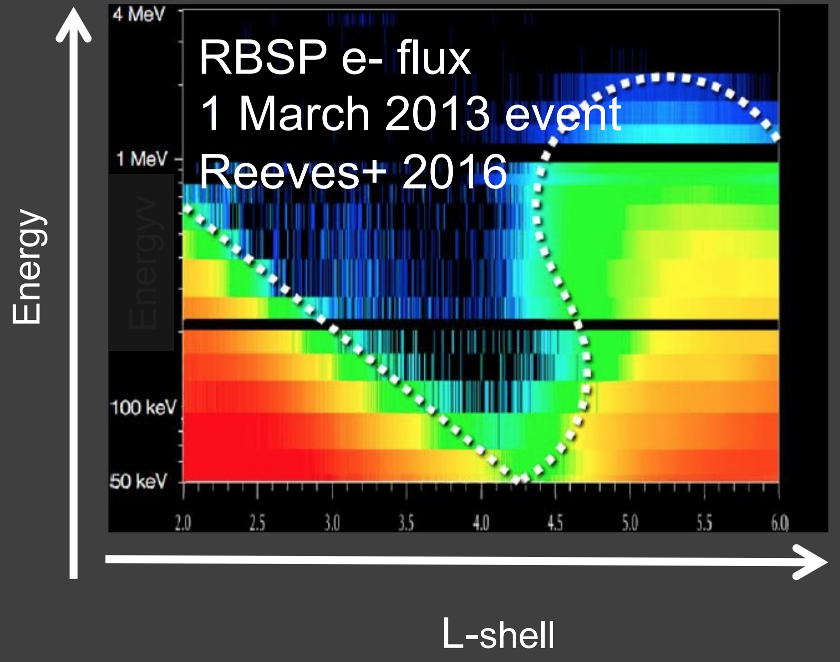

The first full representation of the RB E-Structure from Van Allen Probes (Reeves et al. JGR, 2016)

J.-F. Ripoll, V. Loridan, G. Cunningham, G. Reeves, Y.Y Shprits, *On the Time Needed to Reach an Equilibrium Structure of the Radiation Belts*, JGR, 2015

Radiation belts energy structure (RBSP/MagEIS L2 flux)

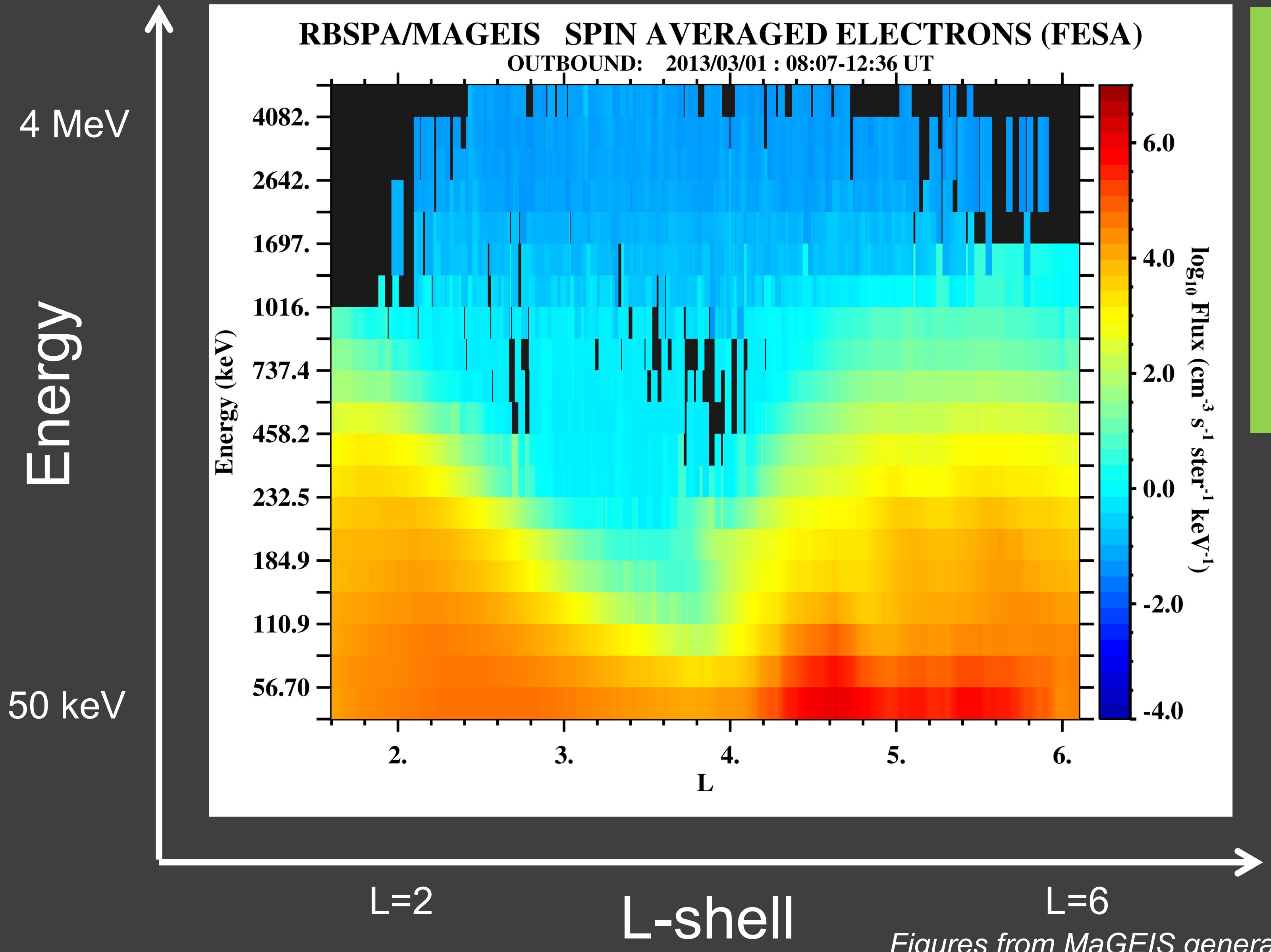

Figures from MaGEIS generated by M. Denton

March 1st
-
March 16th 2013

1 image per 8h

(movie:
3 images/sec
=1day/sec)

Storm times :
March 1st-3rd

Quiet decay:
March 4th-15th

Midnight region

Van Allen Probes Observations (MagEIS Level 2) of the radiation belts energy structure

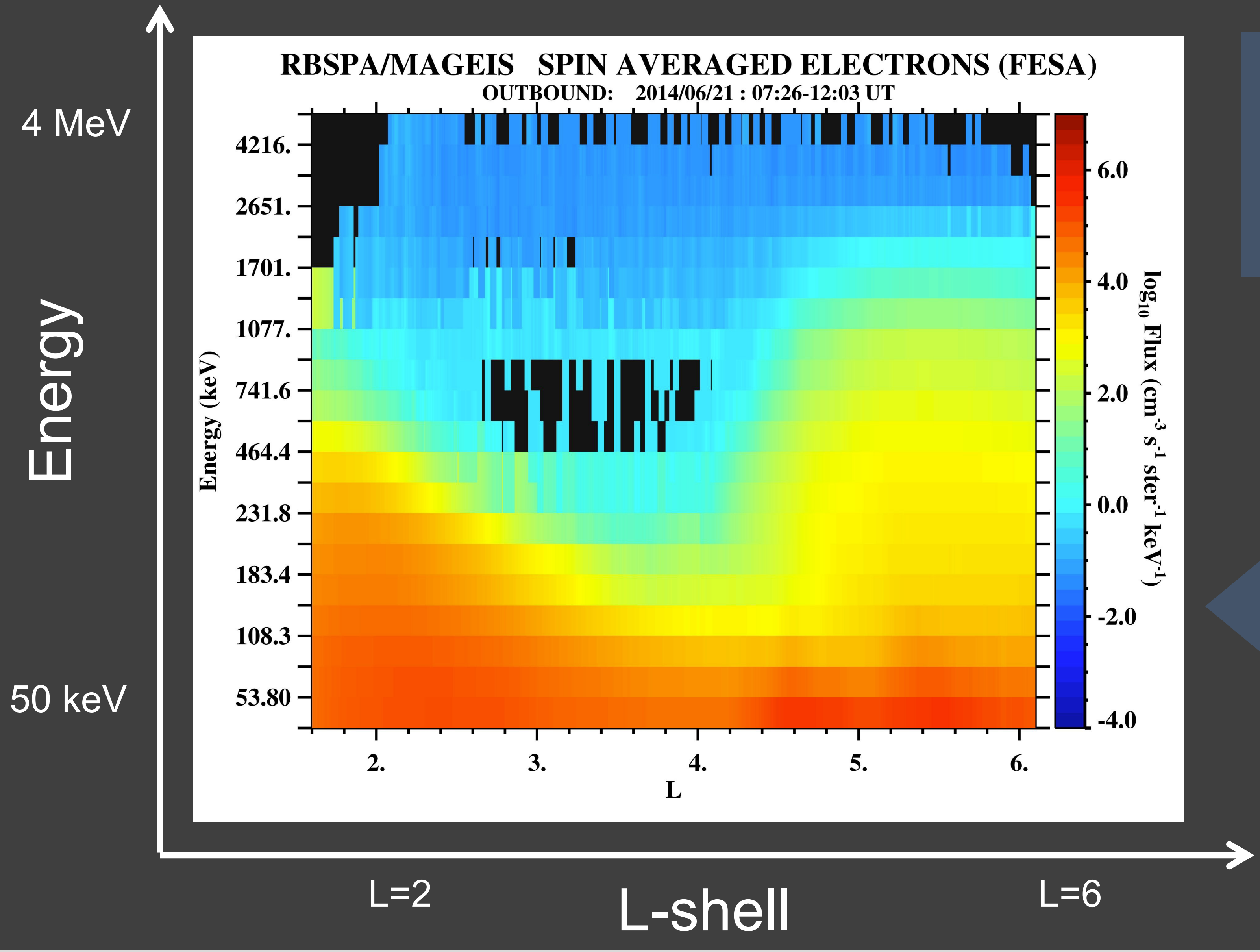

June 21st

-

July 26th 2014

Substorm and HSS injections

- Dynamic injections below 232 keV.
- Substorm injections (e.g. 3rd and 8th)
- ORB with S-shape pattern
- Slot formation
- Gradual outer belt decay

Figures from MaGEIS generated by M. Denton

Fokker-Planck modeling, event-driven wave-particle interactions and simulations of the radiation belts

Hierarchy of Quasi-linear Fokker-Planck models

Fokker-Planck 3D:
The general Fokker-Planck equation for the phase-averaged distribution in a canonical form [Schulz and Lanzerotti, 1974]:

$$\frac{\partial f}{\partial t} = \sum_{i,j=1}^{3} \frac{\partial}{\partial J_i}\left[D_{J_i J_j}\frac{\partial f}{\partial J_j}\right]$$

$$\begin{aligned} J_1 &\equiv \mathcal{M} = \frac{p_\perp^2}{2m_0B} = \frac{p^2\sin^2(\alpha)}{2m_0B}, \\ J_2 &\equiv J = \int_{\Gamma_{\text{bounce}}} p_\parallel \, ds, \\ J_3 &\equiv \Phi = \iint_{\Sigma_{\text{drift}}} \mathbf{B}\cdot d\mathbf{S}, \end{aligned}$$

Codes in use

$$\frac{\partial f}{\partial t} = L^2\frac{\partial}{\partial L}\left(\frac{D_{LL}}{L^2}\frac{\partial f}{\partial L}\right) + \frac{1}{p^2}\frac{\partial}{\partial p}\left(p^2 D_{pp}\frac{\partial f}{\partial p}\right) + \frac{1}{G}\frac{\partial}{\partial \alpha}\left(G D_{\alpha\alpha}\frac{\partial f}{\partial \alpha}\right) + \frac{1}{p^2}\frac{\partial}{\partial p}\left(p^2 D_{p\alpha}\frac{\partial f}{\partial \alpha}\right) + \frac{1}{G}\frac{\partial}{\partial \alpha}\left(G D_{\alpha p}\frac{\partial f}{\partial p}\right) - \frac{f}{\tau_c}.$$

Full Fokker-Planck
VERB-3D
(Y. Shprits' team)

Cross-terms neglected

$$\frac{\partial f}{\partial t} = L^2\frac{\partial}{\partial L}\left(\frac{D_{LL}}{L^2}\frac{\partial f}{\partial L}\right) + \frac{1}{p^2}\frac{\partial}{\partial p}\left(p^2 D_{pp}\frac{\partial f}{\partial p}\right) + \boxed{\frac{1}{G}\frac{\partial}{\partial \alpha}\left(G D_{\alpha\alpha}\frac{\partial f}{\partial \alpha}\right)}$$

Pitch angle equilibrium + neglecting acceleration

1D Reduced Fokker-Planck:

$$\frac{\partial f}{\partial t} = L^2\frac{\partial}{\partial L}\left(\frac{D_{LL}}{L^2}\frac{\partial f}{\partial L}\right) - \frac{f}{\tau}$$

Reduced Fokker-Planck
1D-RFP

Fokker-Planck for this talk:

$$\boxed{\frac{\partial f}{\partial t} = L^2 \frac{\partial}{\partial L}\left(\frac{D_{LL}}{L^2}\frac{\partial f}{\partial L}\right)} \qquad \boxed{+\frac{1}{G}\frac{\partial}{\partial \alpha}\left(G D_{\alpha\alpha}\frac{\partial f}{\partial \alpha}\right)}$$

Radial diffusion + Pitch angle equilibrium

Modeling pitch angle diffusion by wave particle interactions

$$D_{\alpha\alpha} / p^2 = \sum_n \int_{\theta_{\min}}^{\theta_{\max}} D_{\alpha\alpha}^{n,\theta} \sin(\theta) d\theta$$

(Lyons et al. 72)

$$D_{\alpha\alpha}^{n,\theta} = \frac{\pi}{4} \frac{\Omega_c^2}{\gamma^2} \frac{B_{wave}^2}{B_0^2} \left| \frac{c^3}{V_{//}^3} \right| \frac{1}{\cos^3\theta} \frac{\Phi_n'^{\,2}}{\left| 1 - V_g / V_{//} \right|} \frac{g(\theta)}{N(\omega)} \left(\sin(\alpha)^2 + n\Omega_c / \gamma\omega \right)^2 \frac{B^2(\omega)}{\langle B^2 \rangle}$$

Main physical parameters

- >The magnetic field B (dipolar field model) varies as $1/L^3$
- >The electron gyrofrequency varies as $\Omega_e \approx B$
- >The plasma frequency varies as $\omega_{pe} \approx n_e^{1/2}$
- >The electron density varies as $n_e \approx 1/L^4$
- >Wave frequency distribution model $B(\omega) = e^{-\frac{(\omega-\omega_m)^2}{\delta\omega^2}}$ sur $[\omega_{lc}, \omega_{uc}]$
- >Wave power B^2_{wave}
- >Wave normal angle distribution $g_{\varpi}(x = \tan\theta) = e^{-\frac{(x-x_m)^2}{\delta x^2}}$ sur $[x_{\min}, x_{\max}]$
- >At a resonance frequency $k_{//}V_{//} = \omega + n\,\Omega_e / \gamma$

Hiss properties and density from EMFISIS & EFW in March 2013

During quiet times, the plasmasphere extends above L=5.

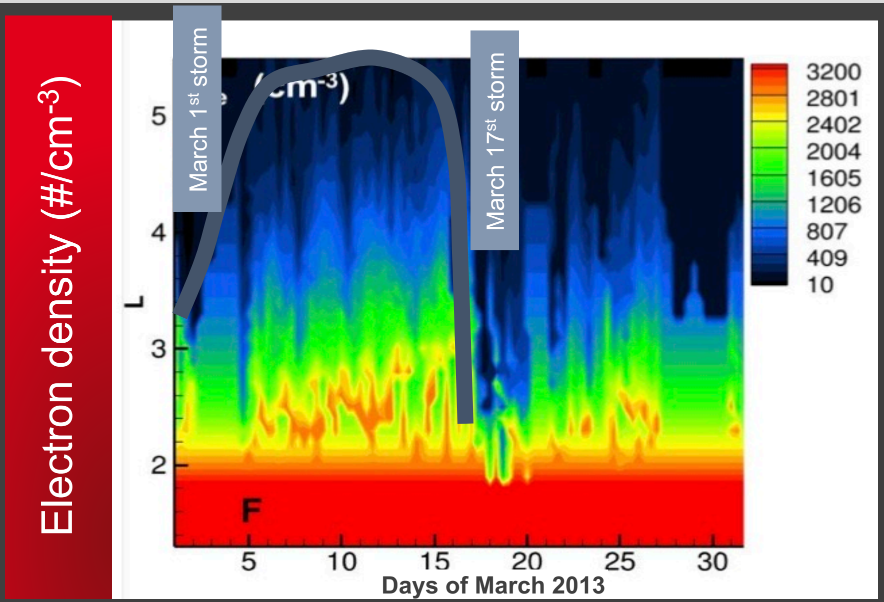

Density EMFISIS (Kurth et al.) and SCC from EFW (S. Thaller, UM)

- Wave frequencies and wave normal angle from EMFISIS (Santolik et al.)
- Amplitudes vary by orders of magnitude, with stronger waves in the plasmasphere (L=2-4)
- MLT-dependence is modeled from Spasojevic et al. 2015

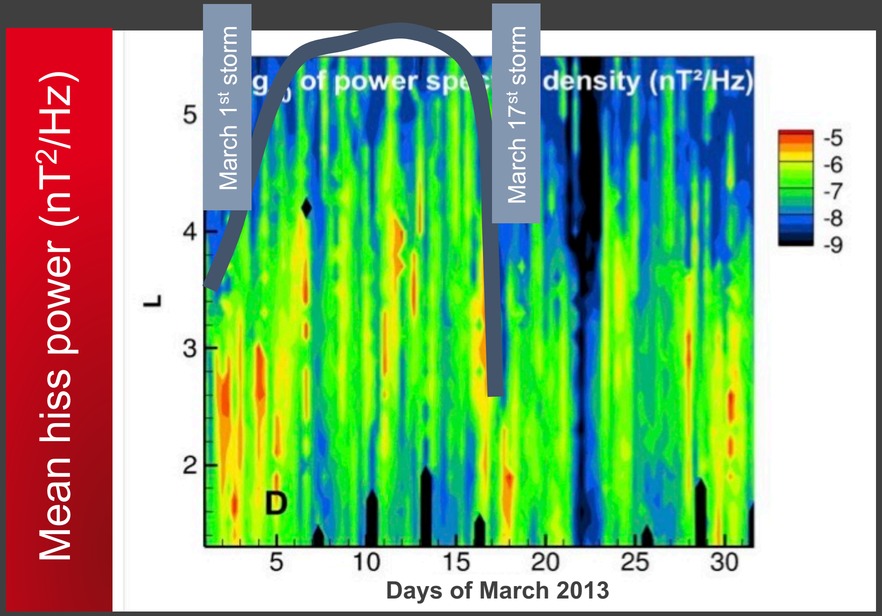

A quite extended plasmasphere favors the existence and the effect of hiss waves

Method for determining event-driven hiss loss

- We compute an event-driven pitch angle diffusion coefficient from all wave/plasma properties from RBSP: 8h resolution, 0.1L. 50 harmonics. Non-//.

8h-resolved

$$D_{\alpha\alpha}(\omega_m \quad \theta_m \quad n_e)$$

Time-averaged

$$\overline{D_{\alpha\alpha}(\omega_m \quad \theta_m \quad n_e)}$$

Not doing

$$\cancel{D_{\alpha\alpha}(\bar{\omega}_m \quad \bar{\theta}_m \quad \bar{n}_e)}$$

From Watt et al. GRL 2021:
- Numerical diffusion experiments are sensitive to variability time scales, even at same time-integrated diffusion
- Experiments reveal more diffusion from average of all diffusion coefficients than when coefficient is constructed from averaged inputs

Pitch angle diffusion coefficients $D\alpha_0\alpha_0$ for 6th of March 2013

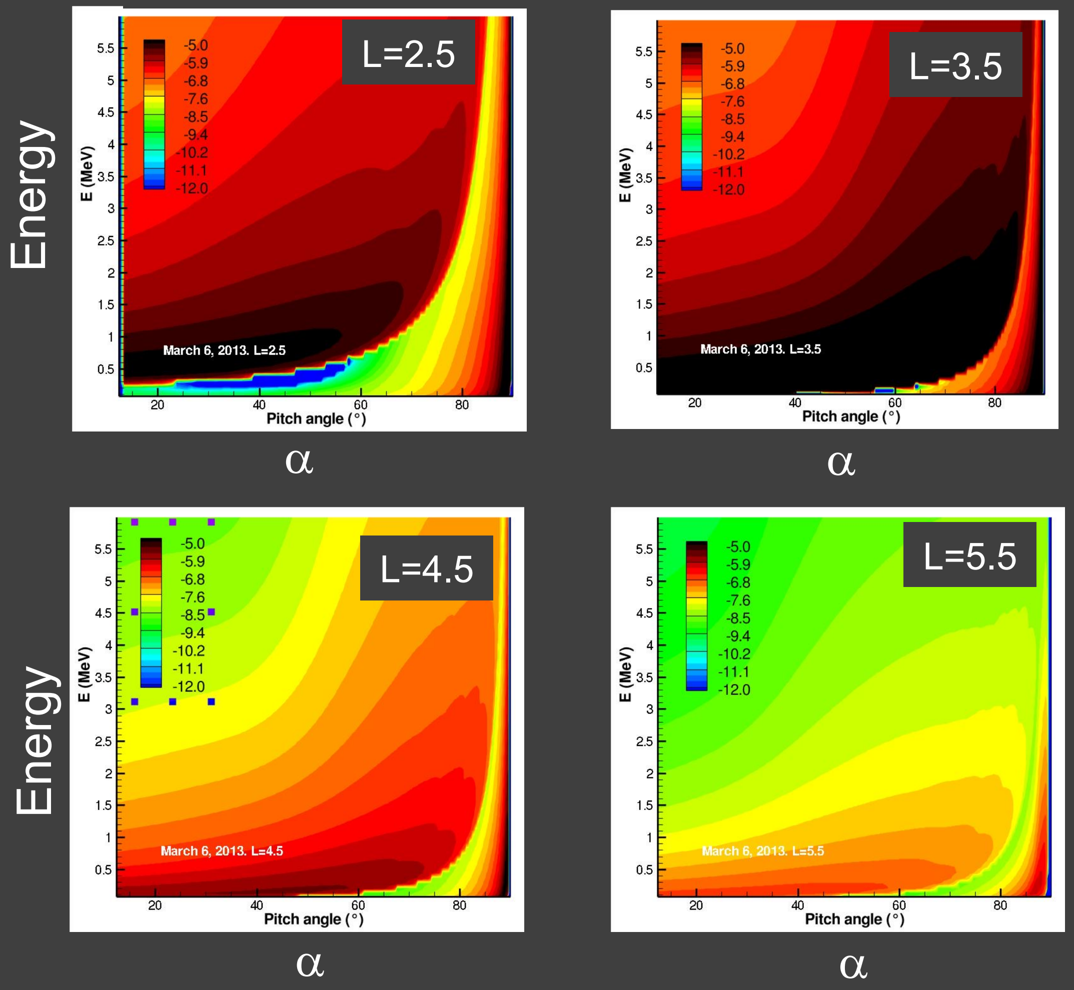

We use the CEA CEVA code (Réveillé, 1997; Ripoll & Mourenas, 2012; Ripoll, Chen, et al., 2014, Ripoll, Reeves, et al., 2016, Ripoll et al., 2017, 2019, 2020)

Massively parallel computations for 6×10^7 $D\alpha_0\alpha_0(L, t, E, \alpha_0)$. (~4 years 1 proc)

10 day averaged $D\alpha_0\alpha_0$ (March 4-15, Kp~1-2) at fixed pitch angle versus (L, E)

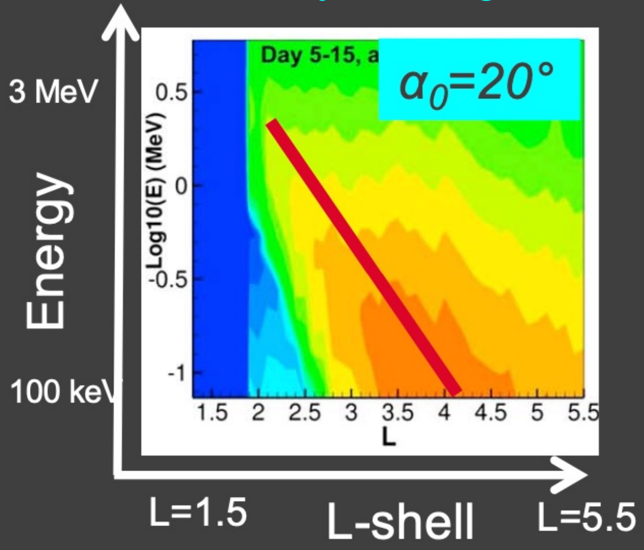

Pitch angle diffusion occurs along a main line in the (L,E) plane that shifts toward higher Lshell as pitch angle increases

J.-F. Ripoll, O. Santolík, G. D. Reeves, W. S. Kurth, M. H. Denton, V. Loridan, S. A. Thaller, C. A. Kletzing, and D. L. Turner, *Effects of whistler mode hiss waves in March 2013,* J. Geophys. Res. Space Physics 122, 2017

10 day averaged $D\alpha_0\alpha_0$ (March 4-15, Kp~1-2) at fixed pitch angle versus (L, E)

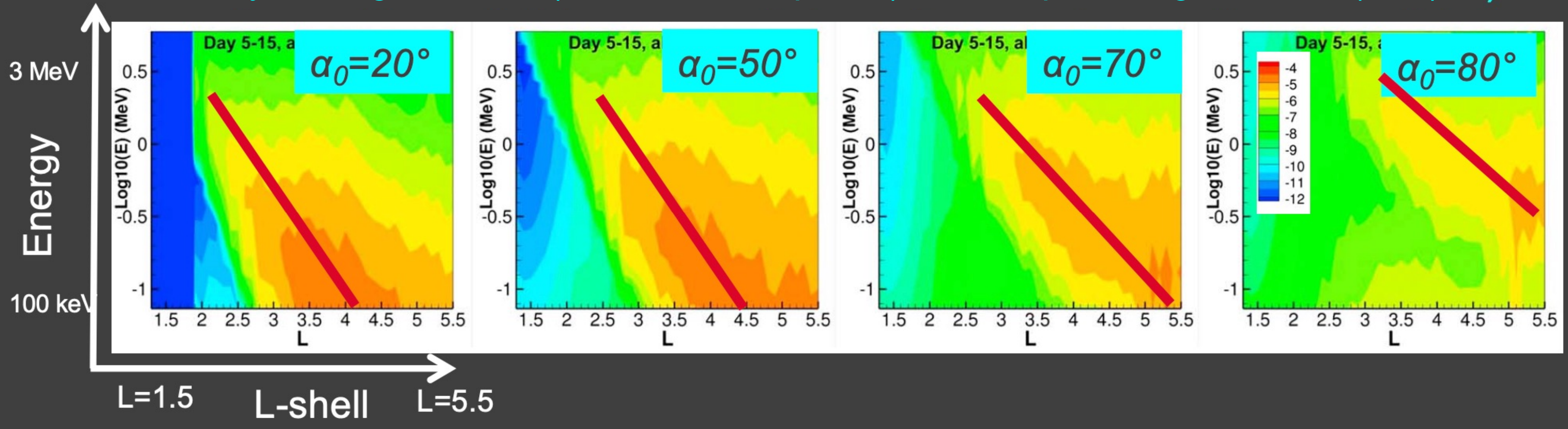

Pitch angle diffusion occurs along a main line in the (L,E) plane that shifts toward higher Lshell as pitch angle increases

J.-F. Ripoll, O. Santolík, G. D. Reeves, W. S. Kurth, M. H. Denton, V. Loridan, S. A. Thaller, C. A. Kletzing, and D. L. Turner, *Effects of whistler mode hiss waves in March 2013,* J. Geophys. Res. Space Physics 122, 2017

Reproducing the 3D radiation belt structure

Van Allen Probes/MagEIS

VERB-3D simulations

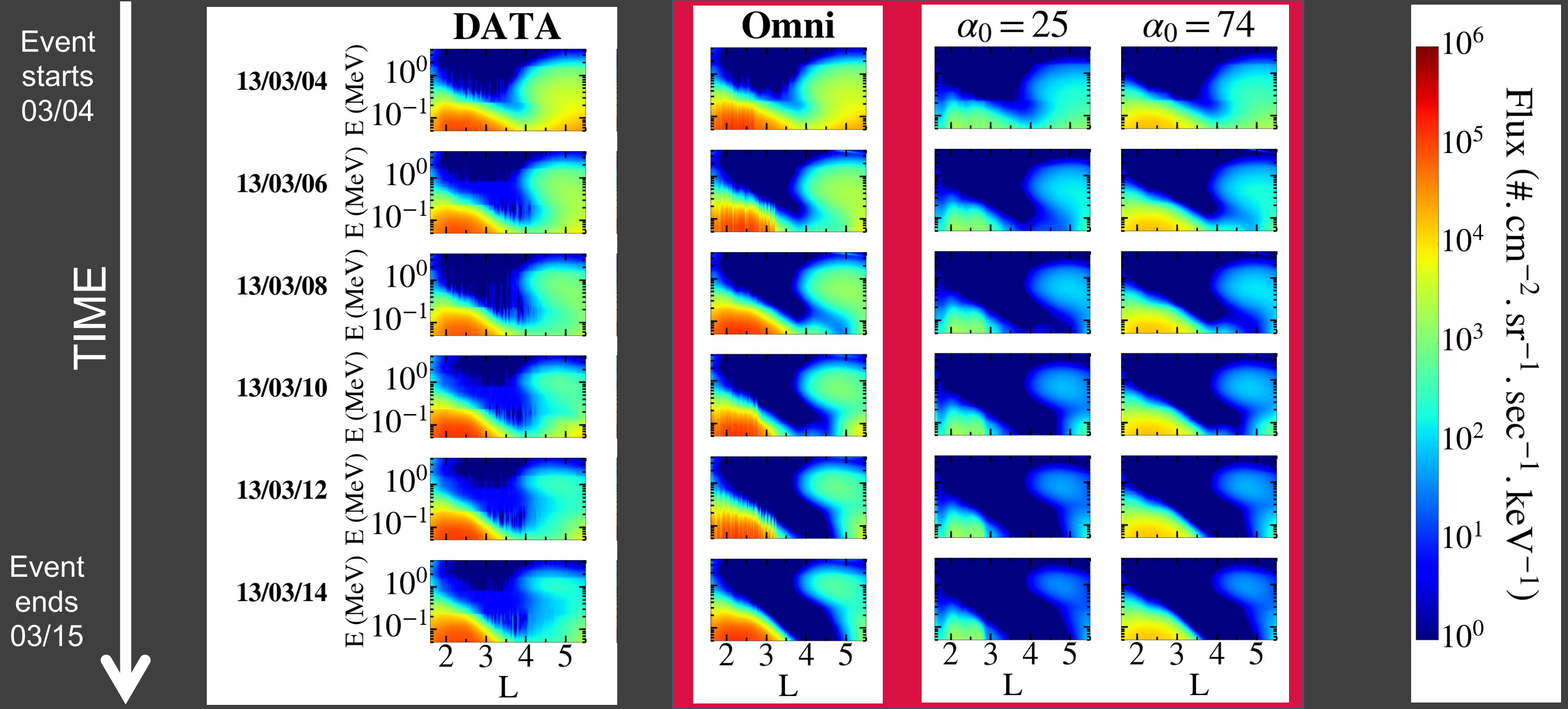

Ripoll+ 2019

- Trapping of high pitch angle electrons at low L
- Relatively isotropic S-shaped outer belt structure
- Narrower inner belt at low p.a. due to 1- proximity with loss cone, 2-pitch angle diffusion affects low pitch angle at low L (small nb of cyclotron harmonics)

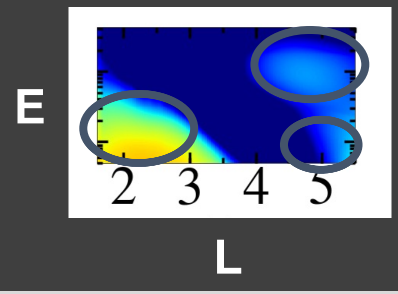

The 3 preserved zones from hiss

- Inner belt
- Outer low energy seed population
- Outer MeV*ich pocket* or *island*

MagEIS L3 observations vs. 3D Fokker-Planck simulations (VERB3D + in house Dαα)

Event starts 03/04

TIME

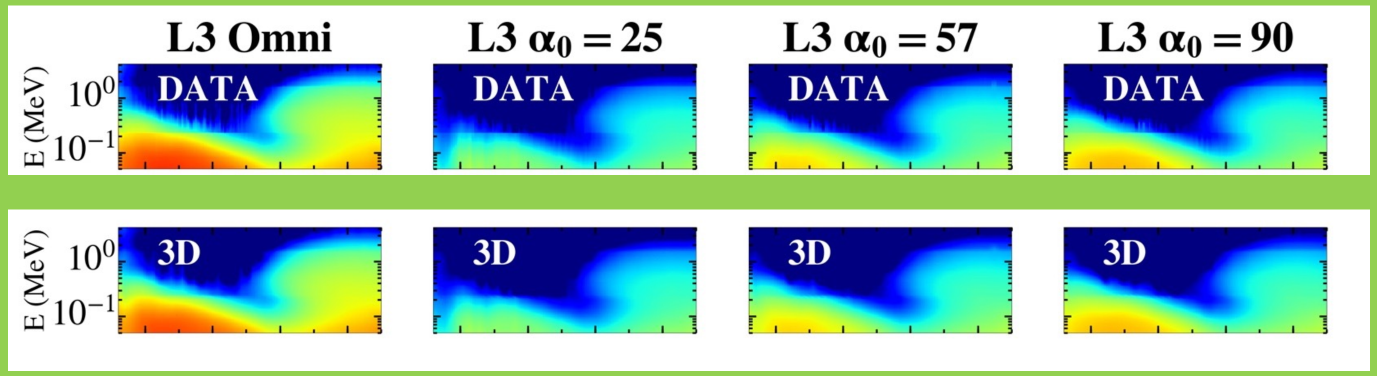

DATA = SIMU

12 days later

Event ends 03/15

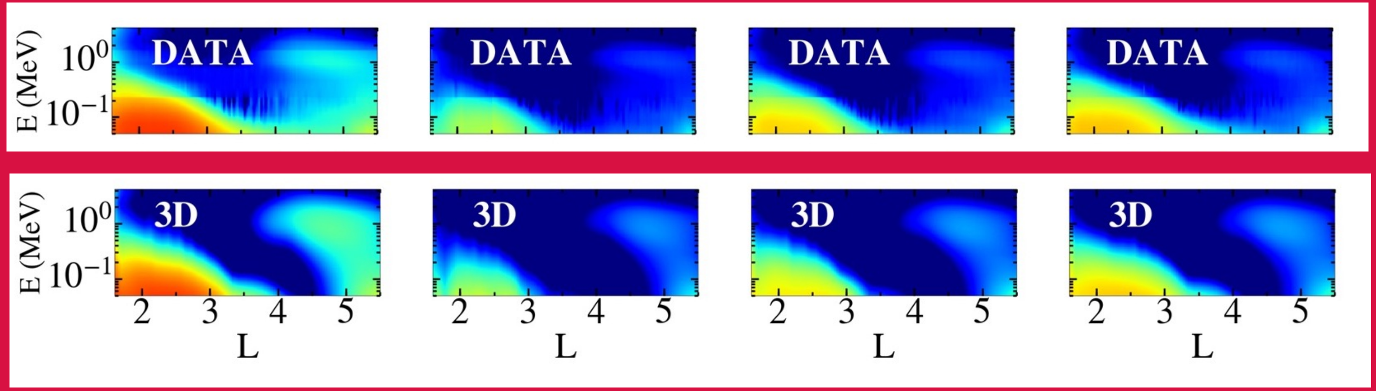

DATA

SIMU

On the dynamic 3D structure from VERB-3D simulations

Omni-Flux

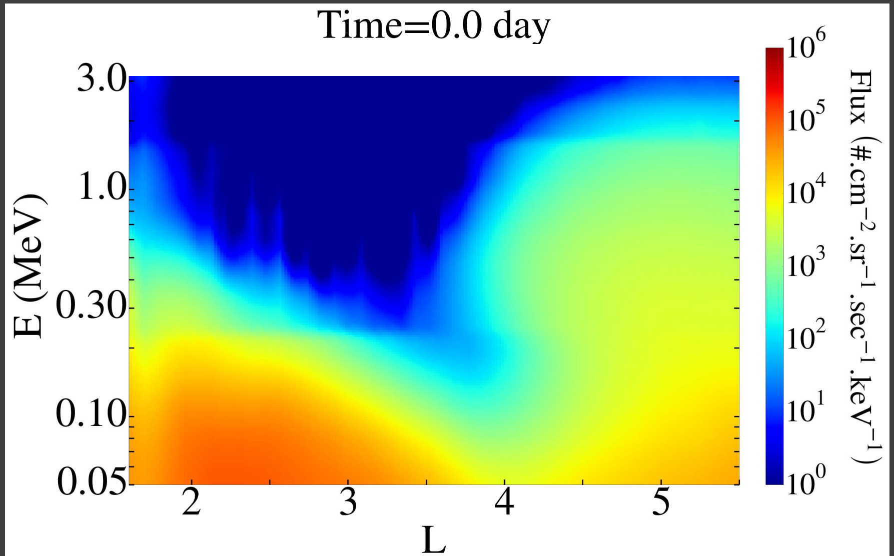

Method

- Solving for RD+PAD from Hiss
- Verb3D-skelleton (v. 2.4.2) for solving radial & p.a. diffusion
- $D_{\alpha\alpha}$ of this work
- BC & IC from MagEIS
- Omniflux is integral of unidir. flux at the latitude of RBSP

Unidirectional Flux

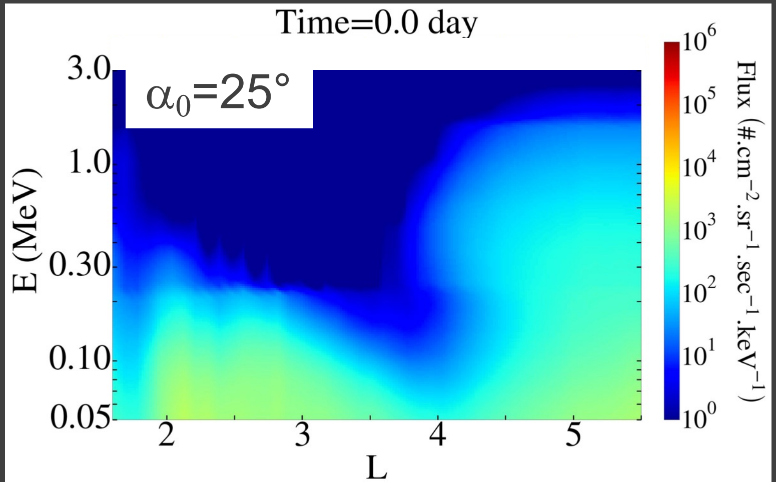

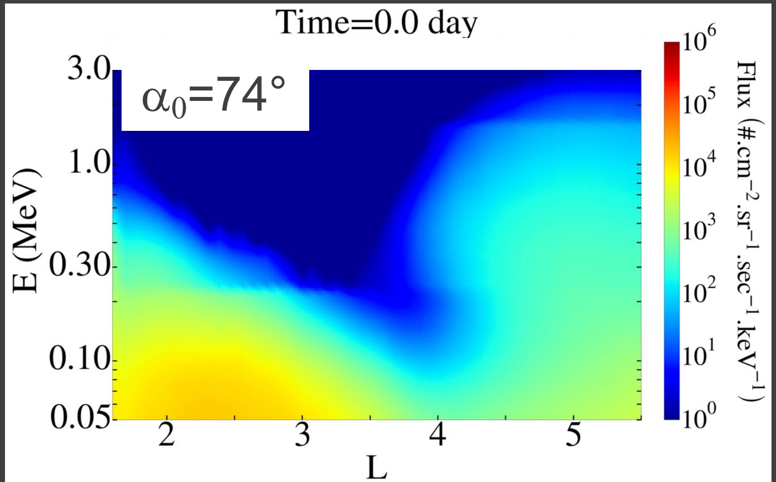

Ripoll+ 2019

Finding some pitch-angle dependence : observations of the theoretical Top-hat PSD

6 conditions to fulfill

1. Wide gradient of $D_{\alpha_0\alpha_0}$ between low-high pitch angles
2. No newly radially inward electrons
3. Dynamics is fast enough to cause significant decays (over ~10 days)
4. Electron levels >> background levels
5. Pitch angle resolution is high enough
6. The s/c latitude allows high pitch angle electrons to be observed.

Where to find it then?
→ at L~[3, 3.5] & E~[100, 300] keV

Simulated Top-Hat PSD
=
Steep observed PSD gradient in p.a.

PSD vs. pitch angle at 4 L-shells

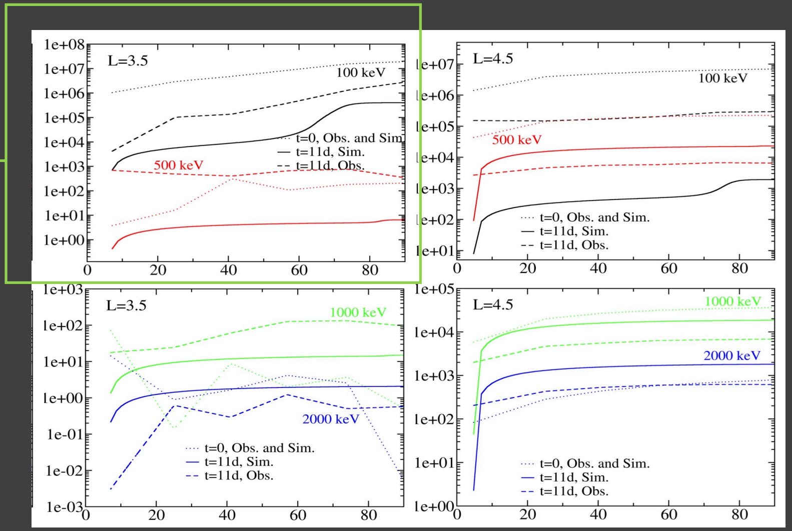

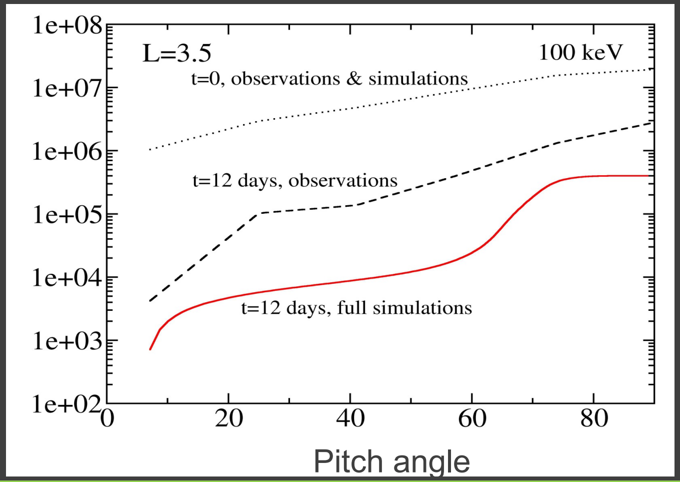

Ripoll+ 2019

Fokker-Planck modeling, event-driven wave-particle interactions and simulations of the radiation belts : scattering in plumes

CEA - www.cea.fr

Effects of hiss in plasmaspheric plumes: intense localized non-equilibrium scattering

- Inject event-driven wave and density properties into Dαα (for the single MLT of the plume)

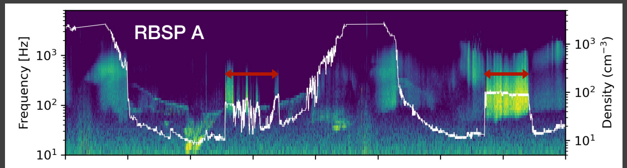

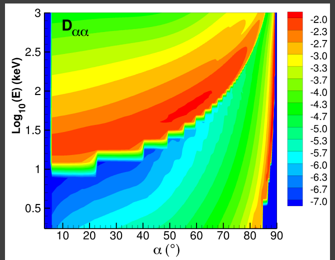

$$\frac{\partial f}{\partial t} = \frac{1}{G}\frac{\partial}{\partial \alpha_0}\bigg|_{L,E}\left(G\widehat{D_{\alpha_0\alpha_0}}\frac{\partial f}{\partial \alpha_0}\bigg|_{L,E}\right)$$

- Intense hiss in the the plume cause fast non-equilibrium scattering

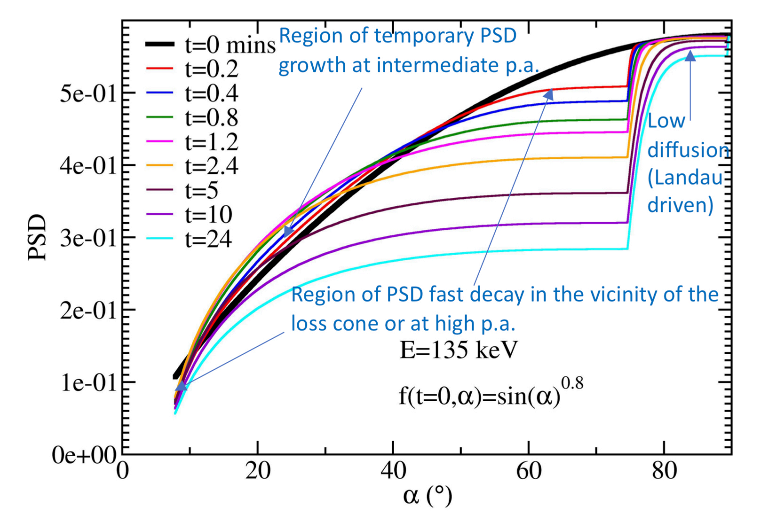

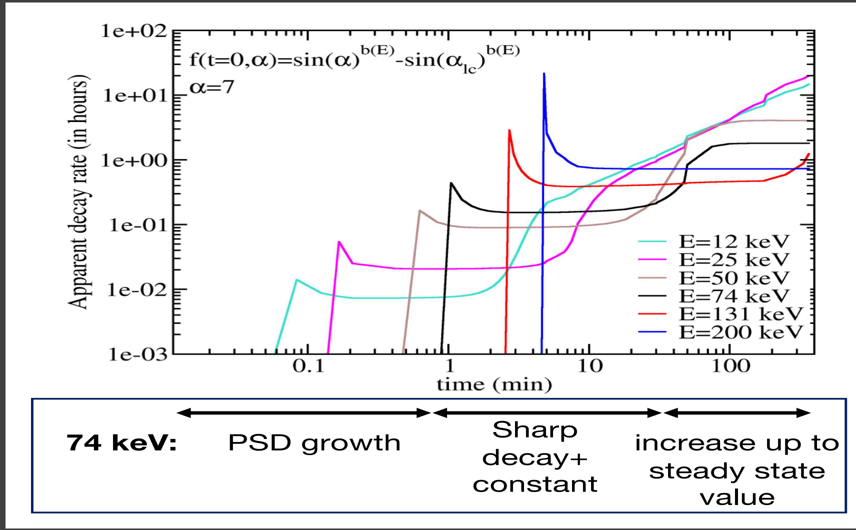

Millan et al., Frontiers, 2021

Conclusions and Perspectives

Summary and Conclusions (1/2)

- **Cold electrons**
  - Density and its level lines (e.g. the plasmapause) are marker/tracer of the geomagnetic activities
  - Fundamental coupling between density and hiss waves
  - The outer electron belt lies within the plasmasphere (40% of all times if counting only Kp<1).
  - 65% of any RBSP data at a given L-shell falls within the plasmasphere, versus 35% in the plasma trough.
  - The plasmasphere through plasmaspheric waves plays an important role in the dynamics of the outer belt

- **Whistlers waves:**
  - Hiss dependence on density. Importance of the coupling for RB simulations
  - Ongoing work to build statistics from RBSP
  - Hiss waves have tremendous effects (WPI) during extended plasmasphere times
  - Hiss sculpt the slot within the belts (L=2 to L=5.5) with typical energy dependence

Summary and Conclusions (2/2)

- **3D L-E-α radiation belts structure is characterized by:**
  - a wider and stronger inner belt at high p.a.
  - a quite isotropic PSD structure in p.a. that decays as p.a. decreases in the outer belt (quiet times)
  - 3 three-zone preserved structure (inner, outer low E seed, outer MeVich remnant island)
- **Successful reproduction of RB energy structure with event-driven wave-particle interaction for:**
  - quiet times (Ripoll et al., 2016, 2019)
  - moderate substorm activity (Ripoll et al., JASTP, 2020)
  - plume driven-loss. (Millan et al., frontiers, 2019)
- **Coupling of plasma and waves improves accuracy of the simulations**

Thank you very much

Thank you: to know more

- Ripoll, J.-F., Claudepierre, S. G., Ukhorskiy, A. Y., Colpitts, C., Li, X., Fennell, J., & Crabtree, C. (2020). *Particle Dynamics in the Earth's Radiation Belts: Review of Current Research and Open Questions*. Journal of Geophysical Research: Space Physics, 125, e2019JA026735.
- Pierrard, V., Ripoll, J.-F., Cunningham, G., Botek, E., Santolik, O., Thaller, S., et al. (2021). *Observations and simulations of dropout events and flux decays in October 2013: Comparing MEO equatorial with LEO polar orbit*. Journal of Geophysical Research: Space Physics, 126, e2020JA028850.
- Ripoll, J.-F., M. H. Denton, D. P. Hartley, G. D. Reeves, D. Malaspina, G. S. Cunningham, O. Santolík, S. A. Thaller, V. Loridan, D. L. Turner, J. F. Fennell, W. S. Kurth, C. A. Kletzing, M. G. Henderson, and A. Y. Ukhorskiy (2020), *Scattering by whistler-mode waves during a quiet period perturbed by substorm activity*, Journal of Atmospheric and Solar–Terrestrial Physics
- Ripoll, J.-F., Loridan, V., Denton, M. H., Cunningham, G., Reeves, G., Santolík, O., et al. (2019). *Observations and Fokker-Planck simulations of the L-shell, energy, and pitch angle structure of Earth's electron radiation belts during quiet times*. Journal of Geophysical Research: Space Physics, 124.
- Malaspina, D. M., Ripoll, J.-F., Chu, X., Hospodarsky, G., Wygant, J. (2018). *Variation in plasmaspheric hiss wave power with plasma density*. Geophysical Research Letters, 45.
- Ripoll, J.-F., O. Santolík, G. D. Reeves, W. S. Kurth, M. H. Denton, V. Loridan, S. A. Thaller, C. A. Kletzing, and D. L. Turner, *Effects of whistler mode hiss waves in March 2013,* J. Geophys. Res. Space Physics 122, 2017
- J.-F. Ripoll, G. Reeves, G. Cunningham, V. Loridan, M. Denton, O. Santolík, W. S. Kurth, C. A. Kletzing, D. L. Turner, M. G. Henderson, A. Y. Ukhorskiy, *Reproducing the observed energy-dependent structure of Earth's electron radiation belts during storm recovery with an event-specific diffusion model* , GRL, 2016
- Ripoll J.-F., Farges, T., Malaspina, D.M., Cunningham, G. S., Lay, E. H. et al. Electromagnetic power of lightning superbolts from Earth to space. Nature Communications 12, 3553 (2021). https://doi.org/10.1038/s41467-021-23740-6
- Ripoll, J.-F., Farges, T., Malaspina, D. M., Lay, E. H., Cunningham, G. S., Hospodarsky, G. B., et al. (2020). Analysis of electric and magnetic lightning-generated wave amplitudes measured by the Van Allen Probes. Geophysical Research Letters, 47, e2020GL087503. https://doi.org/ 10.1029/2020GL087503